Internet of Things 37 (2026) 101933

Contents lists available at ScienceDirect

Internet of Things

journal homepage: www.sciencedirect.com/journal/internet-of-things

Intent-based IoT–Fog HDAF protocol for reliable communication in large-scale industrial iot deployments

Akinyinka Olukunle Akande [a], Kennedy Chinedu Okafor [b,c,d,e,*], Olumide Ajayi [f], Omowunmi Mary Longe [b], Kelvin Anoh [e]

[a] Department of Electrical and Electronics Engineering, Federal University of Technology, Owerri, Nigeria
[b] Department of Electrical and Electronic Engineering Science, University of Johannesburg, Johannesburg 2006, South Africa
[c] Imperial College London, South Kensington Campus, London SW7 2AZ, UK
[d] Department of Engineering, Manchester Metropolitan University, M1 5GD Manchester, UK
[e] School of Engineering, University of Chichester, Bognor Regis, PO21 1HR, UK
[f] Adeleke University Ede, Osun State, Nigeria

ARTICLE INFO

Keywords:
Internet of Things
Intent-based network
Cyber-physical systems
IoT–Fog
Edge computing
Industrial IoT

ABSTRACT

Legacy field protocols such as Fieldbus and HART provide deterministic communication for traditional process control; however, their limited bandwidth, scalability, and adaptability constrain reliable communication in large-scale, data-intensive Industrial IoT (IIoT) systems, particularly under high node density, mobility, and interference conditions. This paper presents a Hybrid Decode–Amplify–Forward (HDAF) protocol within a Fog-assisted cooperative relay architecture to address these limitations. The proposed HDAF scheme adaptively switches between Decode-and-forward (DF) and Amplify-and-Forward (AF) modes under Nakagami-*m* fading, leveraging cooperative Fog relay nodes to enable low-latency, and interference-resilient communication. The framework integrates low-power IEEE 802.15.4 (Zigbee) sensor networks with a 5G New Radio (NR) backhaul via dual-radio IoT–Fog gateways, facilitating traffic aggregation and Quality-of-Service (QoS) mapping. The software-defined coupling mechanism further supports real-time analytics and adaptive relay operation. Validation using theoretical analysis, MATLAB simulations, and field experiments conducted on a gas-processing-plant-inspired industrial testbed demonstrates up to a 95.8% reduction in Bit Error Rate (BER) and approximately 96% improvement in channel capacity compared with non-relay schemes. These results confirm that the proposed IoT–Fog HDAF protocol effectively extends coverage, mitigates interference, and provides a scalable and cost-effective solution for high-reliability, low-latency IIoT communications in dense industrial and 5G-enabled environments.

1. Introduction

Reliable communication in large-scale Industrial IoT deployments remains a fundamental challenge in safety-critical Cyber-Physical Systems (CPS). To address this, we propose an intent-based IoT–Fog hybrid decode–amplify forward (HDAF) protocol that enhances reliability, mitigates interference, and supports deterministic low-latency communication.

* Corresponding author.
E-mail addresses: olukunle.akande@futo.edu.ng (A.O. Akande), kennedy.okafor@mmu.ac.uk (K.C. Okafor), ajayi.olumide@adelekeuniversity.edu.ng (O. Ajayi), omowunmil@uj.ac.za (O.M. Longe), k.anoh@chi.ac.uk (K. Anoh).

https://doi.org/10.1016/j.iot.2026.101933

Available online 25 March 2026

Industrial CPS, including oil and gas pipelines, smart grids, and large-scale process plants, increasingly integrate Internet-of-Things (IoT) sensing, Fog/edge computing, and artificial intelligence-driven analytics to enable real-time monitoring and automated control. In these infrastructures, communication failures caused by interference, fading, congestion, or excessive latency can delay fault detection and lead to severe economic, environmental, and safety consequences. Reliable, interference-resilient, and latency-bounded data delivery between distributed sensors, edge devices, and Fog nodes is therefore essential.

Pipeline monitoring provides a representative example. Pressure, vibration, acoustic, and gas sensors are deployed over extensive geographic areas to detect leaks, mechanical faults, and unauthorised activity. In regions such as Nigeria, Mexico, and the United States, delayed detection of pipeline failures has resulted in substantial economic losses, environmental damage, and safety risks [1–3]. While physical security measures and regulatory interventions remain critical, these incidents also expose a deeper technical weakness: the unreliability of large-scale, interference-prone IoT–Fog communication networks.

IoT-enabled smart infrastructure offers a promising approach for securing such critical assets. Sensor-equipped IoT devices including pressure, vibration, acoustic, and thermal sensors, as well as unmanned aerial systems—can continuously monitor environmental conditions and generate real-time alerts. However, weak security integration, limited bandwidth, reliance on legacy protocols (e.g., Fieldbus and HART), and susceptibility to interference undermine system integrity and reliability [4,5]. These constraints motivate the development of adaptive and intelligent communication frameworks.

From a 3GPP perspective, low-power wireless technologies such as Zigbee (IEEE 802.15.4) are widely adopted in IIoT deployments due to their energy efficiency and low cost [5]. Nevertheless, these networks are constrained in range, data rate, and reliability, particularly in interference-rich or multi-hop industrial environments. To overcome these limitations, Zigbee networks interconnect with 5G systems through IoT–Fog gateways. These gateways function dual-radio, multi-protocol integration nodes, supporting IEEE 802.15.4 at 2.4 GHz on the access side and 5G New Radio (NR) at sub-6 GHz on the backhaul side. They perform protocol translation, traffic aggregation, and quality-of-service (QoS) mapping [5–7]. By leveraging Fog and edge computing, the gateways convert low-rate Zigbee traffic into IP-based streams suitable for transport across the 5G core network, consistent with 3GPP non-3GPP interworking principles. This architecture enables legacy Zigbee devices to benefit from the ultra-reliable, low-latency, and scalable 5G backhaul without modifying their radio interfaces.

Multi-protocol gateway also support interoperability with other non-3GPP technologies such as Wi-Fi and LoRa, providing a flexible and scalable framework for IIoT deployments. Such integration aligns with 3GPP's vision of heterogeneous access convergence and supports reliable, real-time communication for industrial automation, monitoring, and control applications [8,9].

Despite these architectural advances, low-power access networks remain a performance bottleneck. IEEE 802.15.4 networks (e.g., Zigbee) operate at approximately 250 kbps, limiting their suitability for data-intensive applications [10]. In multi-hop, interference-rich conditions, throughput may decrease to 50–200 kbps. Latency can range from tens to several hundred milliseconds, far exceeding the 10–20 ms requirement for mission-critical CPS [11]. Bit error rates (BER) may reach 10^{-2}–10^{-3} without advanced error control, whereas industrial CPS typically require BER levels of 10^{-5} or lower to ensure deterministic performance [10,11]. This persistent performance gap motivates the need for adaptive, interference-resilient cooperative relaying mechanisms such as the proposed IoT–Fog HDAF protocol.

Intent-based Fog-enabled relay architectures address these challenges by integrating edge processing, extended coverage, and enhanced signal robustness. This approach provides scalability and cost efficiency for real-time industrial monitoring [12,13]. Intent-based management (IBM), originally developed in software-defined networking (SDN), introduces an abstraction layer that simplifies orchestration in complex IoT–Fog environments. The Internet Research Task Force (IRTF) formally defined an intent in 2015 as "an abstract, high-level policy to operate a network" [12]. In practice, intents encode service requirements—such as reliability, throughput, or latency—allowing networks to adapt dynamically to operational conditions [13].

Cooperative relaying further improves IoT–Fog performance by extending connectivity, improving reliability, and mitigating signal degradation in dynamic or obstacle-rich environments [14]. Conventional relaying schemes, including amplify-and-forward (AF), decode-and-forward (DF), adaptive relaying (AR), and fixed relaying (FR), suffer from noise amplification, decoding failures, and performance degradation under interference-rich conditions [14–16]. Many existing models assume idealised channel conditions and overlook multipath fading, mobility-induced variations, and channel obstructions typical of industrial deployments [17]. Although prior studies have examined outage probability, symbol error rate, and hybrid relaying strategies [14–17], they often rely on simplified assumptions that fail to capture large-scale IoT–Fog complexity. This limitation is critical because task offloading in massive IoT–Fog networks under realistic conditions must account for interference, path loss, and signal attenuation, which remain largely unaddressed [16]. Location-aided maximal ratio combining (LMRC) has been investigated to mitigate fading and interference, but its integration within cooperative relaying frameworks remains limited and largely focused on 5G New Radio (NR) deployments [18,19].

While [20] addresses Internet of Vehicles (IoV) security using lightweight cryptography and deep-learning-based anomaly detection, our work focuses on physical- and network-layer performance optimisation. Similarly, [21] applies deep learning for generic network intrusion detection; in contrast, our approach designs an IoT–Fog HDAF communication protocol that leverages cooperative Fog relays and software-defined control to enhance link reliability, channel capacity, and deterministic data delivery in interference-limited industrial environments.

To overcome these limitations, we propose the Smart Intent-Based Fog-IoT Relay Network (SIF-IRN), a hierarchical IoT–Fog architecture in which service intents guide relay selection and operation. The framework supports hybrid AF/DF relay selection based on service objectives, channel conditions, and network state, enabling reliable and low-latency packet delivery with bounded latency. Under Nakagami-m fading, the HDAF protocol integrates cooperative Fog relay nodes with non-invasive sensors via software-defined coupling (SDC), dynamically switching between decoding and amplification according to real-time channel quality. This mechanism reduces edge congestion, adapts to environmental variability, and supports intelligent task offloading.

The proposed protocol significantly improves BER, channel capacity, and coverage under realistic deployment conditions. We validate the approach through analytical modelling, dynamic DF/AF relay selection, MATLAB simulations, and a physical testbed using TelosB motes. Performance metrics including BER, latency, energy efficiency, and throughput confirm robustness in indoor and outdoor industrial scenarios, including interference-rich environments and mobility up to 100 m.

The main contributions of this paper are:

- Real-world deployment of an intent-based IoT–Fog sensing infrastructure at a gas plant using TelosB sensor nodes.
- Design of the IoT–Fog HDAF protocol integrating location-based MRC for adaptive hybrid relaying.
- Analytical modelling of cooperative relay systems under Nakagami-*m* fading channels.
- Demonstration of BER reduction and channel-capacity gains, achieving up to 95.8% improvement over conventional relay.
- Enhanced throughput under high SNR and multi-relay configurations, reducing reliance on dense small-cell deployments.
- Practical insights for scalable IIoT deployment, improving interference mitigation, and spectral efficiency.

The remainder of the paper is organised as follows: Section 2 reviews related work; Section 3 presents the system model; Section 4 introduces the system algorithm; Section 5 describes the experimental IoT–Fog use case; Section 6 presents performance analysis; Section 7 concludes the paper.

2. Related works

This section reviews cooperative relaying strategies in IoT–Fog networks, focusing on existing approaches to relaying, relay selection, and network optimisation. While these studies provide valuable insights, current solutions often rely on ideal channel assumptions, centralised control, or static traffic conditions, limiting their applicability in dense, heterogeneous, and interference-prone IoT–Fog environments. These limitations motivate the development of the HDAF protocol.

2.1. Cooperative relaying in IoT–Fog networks

Prior research has explored opportunistic relaying, Adaptive Relaying (AR), Fixed Relaying (FR), Amplify-and-Forward (AF), and Decode-and-Forward (DF) protocols for enhancing coverage, reliability, and capacity in IoT–Fog networks. Each approach, however, has inherent drawbacks. AF relays amplify both signal and noise, reducing effective SNR under poor channel conditions, while DF relays can fail when decoding errors occur, leading to packet loss and retransmissions [22,23]. Cooperative communication and diversity techniques improve connectivity in dense deployments but often assume static channel conditions and ideal relay behaviour, failing to account for mobility, interference, or real-time QoS requirements [23].

2.2. Relay selection and machine learning approaches

Intelligent relay selection using Markov Decision Process (MDP) or Deep Reinforcement Learning (DRL) has shown performance gains in cooperative DF and Non-Orthogonal Multiple Access (NOMA) systems, improving outage probability, BER, and spectral efficiency compared to classical AF/DF schemes [18,22]. Despite these advantages, existing learning-based solutions often rely on extensive training datasets, centralised decision-making, or static network topologies, limiting their adaptability in dynamic IIoT or vehicular environments where node density, interference, and channel conditions fluctuate rapidly.

2.3. Network challenges and small-cell deployments

Emerging industrial IoT applications—including real-time AR, autonomous vehicle telemetry, and high-definition sensor analytics place high demands on low-latency, high-throughput networks [17]. Previous studies have explored hybrid relays over Nakagami-*m* channels to enhance reliability [17]. Nevertheless, dense small-cell deployments continue to face significant challenges, including co-channel interference, mmWave propagation limitations, energy consumption, and hardware deployment costs [24,25]. The growing number of mobile devices further stresses base stations, highlighting the need for cooperative and adaptive communication strategies that maintain QoS under realistic network conditions [26].

2.4. Relaying protocols and network performance

Various relaying protocols, including quantize-and-forward (QF), AF, DF, and hybrid schemes with simultaneous wireless information and power transfer (SWIPT) techniques, have been investigated to improve throughput and reliability in IoT–Fog networks [22,23]. While these approaches mitigate signal degradation and interference, they generally rely on fixed relay selection or assume idealised channel conditions. Consequently, latency, energy efficiency, and scalability remain critical limitations in dynamic, interference-rich industrial IoT environments [25].

2.5. Limitations of authentication and data-sharing frameworks

Several authentication and secure data-sharing frameworks for 5G-enabled vehicular Fog systems have been proposed, including

Chebyshev-polynomial-based authentication, anonymous authentication (ANAA-Fog), chaotic-map-based privacy preservation (CM-CPPA), password-guessing-resistant key agreements, RSU-free schemes, and certificateless ECA-VFog protocols [27–29]. While these methods ensure low-latency, privacy-preserving access, they inherently assume a reliable underlying communication layer and do not account for physical-layer impairments such as fading, interference, relay failures, or mobility-induced packet loss [30–32]. Therefore, these security-centric frameworks alone cannot guarantee the low-BER, low-latency, and interference-resilient communication required for robust IoT–Fog operations. Table 1 provides a systematic comparison of these protocols, highlighting their constraints and motivating the need for an adaptive, intent-driven HDAF framework. This addresses these gaps by combining adaptive cooperative relaying with intent-based orchestration, thereby ensuring reliable, low-latency, and interference-resilient communication for secure vehicular and industrial IoT–Fog applications beyond the capabilities of existing security- or protocol-centric approaches.

2.6. Research gaps and motivation

Despite extensive research on cooperative relaying and network optimisation, several critical gaps remain in IoT–Fog deployments. Conventional AF and DF protocols suffer from noise amplification and decoding errors, while Amplify-and-Relay (AR) and Forward-and-Relay (FR) schemes lack adaptability in interference-rich, dynamic IoT–Fog environments [17–23]. Intelligent relay selection strategies, including Deep Reinforcement Learning (DRL) and Markov-based approaches, primarily optimise outage probability and BER but do not fully address large-scale task offloading, heterogeneous traffic, and mobility-induced variations in industrial networks [18,22].

Similarly, 5G New Radio (NR) small-cell deployments, while capable of high data rates and low latency, remain constrained by co-channel interference, energy inefficiency, and limited mmWave coverage in obstructed industrial environments [23–25]. Techniques such as quantize-and-forward (QF), power splitting (PS), time switching (TS), and simultaneous wireless information and power transfer (SWIPT) provide interference mitigation and energy harvesting benefits [22,23] but are often implemented in isolation without a unified framework capable of jointly managing coverage, reliability, and energy efficiency. These limitations highlight the need for a robust, adaptive, and hybrid relaying protocol that simultaneously improves coverage, mitigates interference, optimises energy usage, and supports reliable task offloading in dense IoT–Fog networks.

Collectively, prior studies expose two critical gaps:

- **Communication-layer limitations**: Existing AF, DF, SWIPT, NOMA, and DRL-based schemes inadequately address real-world fading, interference, mobility, and energy efficiency.

Table 1
Summary of limitations of existing protocols.

Ref	Technique	Channel model	AI/ML	Energy consumption	Latency	Key limitations
AF (Al-Kahtani et al.,2020) [33])	AF	Rayleigh	No	High	Medium	Amplifies noise along with signal, leading to SNR degradation and reduced BER performance under low SNR conditions [3]: (amplifies noise and interference)
DF (Lucero et al., 2023) [34]	DF	Nakagami	No	Medium	Medium	Decoding failures: Higher processing complexity and latency; performance relies on correct decoding at the relay, which may not always be possible in severe fading [3,4],.
SWIPT (Song et al., 2024) [35]	SWIPT	Rician	No	High power consumption	High	Excessive computational complexity and signaling overhead lead to increased latency, energy consumption, and reduced spectral efficiency, thereby limiting the practicality of advanced relay protocols in real-world deployments.
NOMA (Tran et al., 2025) [36]	NOMA	Log-normal	Partial	High	medium	Successive Interference Cancellation (SIC): While SIC-based relay schemes can separate multiple overlapping signals and improve spectral efficiency, their high computational complexity, energy consumption, and error propagation make them less suitable for low-power, low-latency cooperative networks. In contrast, the proposed HDAF protocol achieves adaptive relay performance without relying on SIC.
DRL-Relay (Kim et al., 2023; [37,38] Qian et al. (2025)	DRL	Fading	Yes	High	medium	Learning overhead in DRL-based relay schemes significantly increases both energy consumption and end-to-end latency due to continuous training, exploration, and excessive signaling
Proposed HDAF	Hybrid DF/AF	Nakagami	Yes (Intent-based)	Low/Adaptive	Low	Unlike DRL-based approaches, the proposed HDAF protocol achieves adaptive performance without incurring learning overhead, making it suitable for real-time cooperative networks. By avoiding such overhead, the protocol attains lower latency and improved energy efficiency while maintaining high reliability.

- **Security-centric frameworks' reliance on ideal channels:** Many authentication and data-sharing approaches presume reliable wireless links, ignoring physical-layer impairments that dominate industrial IoT and vehicular Fog environments.

To bridge these gaps, we propose the HDAF protocol integrated with intent-driven Fog orchestration. By combining adaptive cooperative relaying with dynamic forwarding schedules, SNR-aware mode selection, and Fog-assisted QoS mapping, HDAF ensures low-latency, interference-resilient, and energy-efficient communication. Unlike conventional relay or security-focused schemes, HDAF is designed for practical deployment in dense, heterogeneous IoT–Fog networks, supporting industrial automation, real-time monitoring, and vehicular cyber-physical systems.

3. System model

To address the limitations of existing cooperative relaying strategies, this work introduces the HDAF protocol integrated within the SIF-IRN framework. Unlike conventional AF, DF, or isolated optimisation schemes, HDAF dynamically switches between decoding and amplification based on instantaneous channel conditions, ensuring robust, low-latency communication under fading, interference and mobility. The SIF-IRN framework provides intent-driven orchestration across distributed edge and Fog nodes, unifying interference mitigation, coverage extension, and energy optimisation. Fog nodes leverage high-level service intents to manage AI inference, orchestrate edge tasks, and proactively adjust network behaviour, reducing congestion and latency in large-scale IoT–Fog deployments. Within this framework, HDAF enables cooperative relay operations that jointly optimise BER, channel capacity, and energy efficiency. By integrating adaptive relaying with SIF-IRN orchestration, the system overcomes the key gaps of conventional AF/DF protocols, DRL- or MDP-based relay selection, and small-cell deployments, providing resilient, high-performance communication for dense, heterogeneous IoT–Fog networks.

3.1. Design architecture

Fig. 1 illustrates the analytical modelling of AF, DF, and HDAF relay protocols within an AirComputation (AirComp) framework [21]. The source signal is modulated using binary phase shift keying (BPSK) and quadrature phase shift keying (QPSK) at the

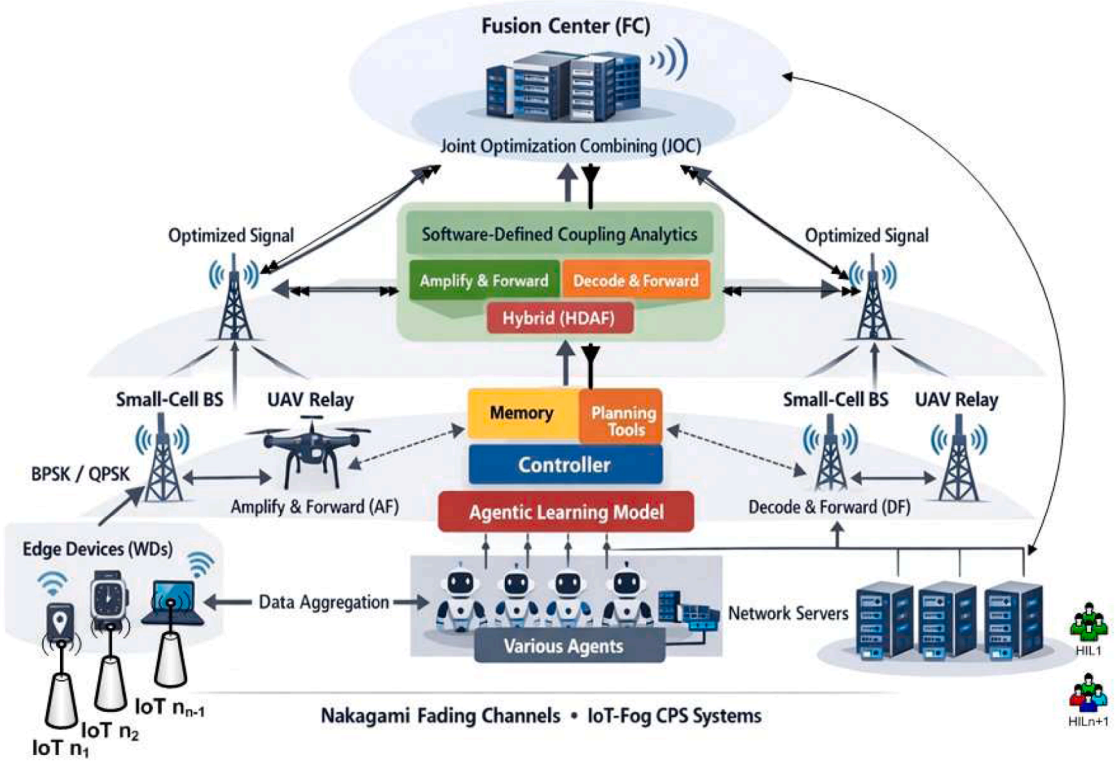

Fig. 1. Hierarchical AirComp architecture employing multiple relays (small-cell base stations and UAVs) to aggregate data from edge wireless devices (WDs) to a fusion centre (FC) for in-network computation. The framework integrates AF, DF, and HDAF protocols, augmented by the SDCA module. In a two-phase relay scheme, WDs transmit modulated baseband signals (BPSK/QPSK) to fog relays, which forward optimised signals to the FC for aggregation via JOC using a matched filter. The architecture supports heterogeneous aerial–terrestrial networks under Nakagami fading channels, enabling advanced IoT–Fog CPSs.

transmitter and demodulated at the receiver to maintain high signal fidelity. Mathematical models of the relay protocols are embedded into the system to evaluate cooperative behaviour, interference mitigation, and energy efficiency under realistic network conditions. At the receiver, signal quality is enhanced using the joint optimisation combining (JOC) MIMO technique with a matched filter (MF), which maximises the signal-to-noise ratio (SNR) and provides resilience against fading and interference. The HDAF protocol is evaluated using BER, CC, throughput, and outage probability metrics under varying SNR conditions over Nakagami fading channels. Extensive simulations demonstrate that HDAF integrated into SIF-IRN enables reliable 2.4 GHz connectivity, intelligent task offloading, and energy-efficient communication for advanced IoT–Fog networks and cyber-physical systems (CPS).

As shown in Fig. 1, the agentic AI framework is modelled as a hierarchical multi-agent system embedded within the AirComp architecture. Edge wireless devices (WDs) operate as sensing agents whose data are aggregated via small-cell base stations and UAV-based fog relays to the fusion centre (FC). An agentic learning model equipped with memory, planning tools, and a central controller coordinates multiple specialised agents interacting with network servers to optimise aggregation and computation tasks. Within this framework, AF, DF, and HDAF relay agents autonomously select appropriate forwarding protocols based on channel conditions under Nakagami fading. Using agentic planning and reasoning, the framework dynamically determines relay mode selection, signal amplification level, and computation policy to support JOC with matched filtering at the FC.

The Software-Defined Coupling Analytics (SDCA) module further enhances autonomous decision-making by enabling cross-layer optimisation between aerial and terrestrial relay tiers. The agentic AI system learns from network experience through continual interaction with heterogeneous aerial–terrestrial nodes, enabling adaptive aggregation accuracy, latency control, and robustness. Cooperating agents communicate with network servers and fog relays, allowing routing, protocol switching, and computation offloading to be autonomously configured. This integration of agentic AI with hierarchical AirComp supports advanced IoT–Fog CPSs by enabling self-configuring, self-optimising, and resilient in-network computation.

3.2. Software-defined coupling analytics (SDCA)

Building on the system architecture in Section 3.1, the SDCA module serves as the orchestration layer that enables adaptive intelligence across the relaying system. Within the AirComp framework, multiple relays—including UAV drones and ground-based small-cell base stations—assist the FC in aggregating data from edge WDs. Relay operation follows a two-step process:

- Edge WDs transmit data to Fog relays.
- Relays apply AF, DF, or HDAF before forwarding signals to the FC, where lateral combined decoders aggregate data efficiently.

The SDCA module dynamically coordinates these processes to ensure resilience and performance under diverse network and channel conditions. Its core functions include:

- Dynamic relay protocol selection: Analyses real-time SNR, BER, fading severity (Nakagami), and interference to switch adaptively between AF, DF, and HDAF, minimising outage and maximising throughput.
- Adaptive signal processing: Tunes BPSK/QPSK modulation and optimises JOC with MF by adjusting MIMO weights for diversity gains, while using predictive models to forecast relay performance.
- Cross-layer coupling analytics: Integrates PHY-layer metrics (e.g., channel quality, fading) with network-layer parameters (e.g., latency, throughput, reliability), supported by feedback loops for power adjustment, coding, and relay cooperation.
- Multi-relay and multi-cell coordination: Jointly manages UAV and ground relays, coupling streams from multiple WDs for AirComp aggregation while reducing redundancy before FC aggregation.
- AI-driven optimisation and resilience: Uses machine learning to enhance predictive relay optimisation and system robustness across heterogeneous IoT–Fog CPS networks.

By embedding these functions, SDCA ensures that HDAF operates as part of a coordinated, intelligent system capable of real-time adaptation and efficient resource management in dense IoT–Fog deployments. The focus of this work is an intent-based HDAF protocol for improving reliability and reducing BER in fog-enabled IoT networks. The protocol is deployed in a real-world testbed at SPDC's gas plant using Zigbee-compliant TelosB motes and evaluated under Nakagami fading conditions.

3.3. Massive IoT-Fog task offloading

With the established architecture and the orchestration role of SDCA in Fig. 1, we now detail the breakdown of the system model for Massive IoT-Fog task offloading from the edge layer.

3.3.1. Fog-offloading amplify-forward (AF) relay system

At the edge layer, the cooperative communication system consists of the information Source S, the Relay R, and the Destination D. The relay communicates in half-duplex with a single antenna, and the complete broadcast of the signal information in different directions takes place in two phases. In phase one, the source broadcasts its message directly to both the relay device and the destination node. The instantaneous signal-to-noise ratio (SNR) of the transfer symbol is expressed as; [39]

$$\mathscr{Y}_{s,r_1} = \sqrt{\mathscr{P}_s}\, h_{s,r_1}\, \mathscr{X}_\tau + \mathscr{Z}_{s,r_1}, \tag{1}$$

$$\mathscr{Y}_{s,d} = \sqrt{\mathscr{P}_s}\, h_{s,d}\, \mathscr{X}_\tau + \mathscr{Z}_{s,d} \tag{2}$$

where, $\mathscr{Y}_{s,r_1}$ is the output SNR from the source to the relay, $\mathscr{Y}_{s,d}$ is the SNR from the source to the destination. $h_{s,r}$ and $h_{s,d}$ are the channel gains in the Nakagami fading environment between the $S \rightarrow R$ and $S \rightarrow D$, $\mathscr{P}_s$ is the transmission power, and $\mathscr{X}_\tau$ is the transmitted symbol. The terms $\mathscr{Z}_{s,r_1}$ and $\mathscr{Z}_{s,d}$ denote zero-mean additive white Gaussian noise (AWGN), with unit variance at the first relay and destination, respectively.

The AF relay protocol amplifies the transmitted symbol and forwards it to the destination to compensate for signal loss due to channel obstruction and signal attenuation from the source and relay. The relay protocol implements this with the help of the signal amplifying factor, $\mathscr{K}_r{}^{(AF)}$, and is expressed as;

$$k_r{}^{(AF)} = \frac{\sqrt{P}}{\sqrt{P\left|h_{s,r}\right|^2 + 1}} \tag{3}$$

where, $\mathscr{K}_r{}^{(AF)}$ is the AF amplifying factor, and $\mathscr{P}$ is the amplifying power.

In phase 2, the amplified source signal from the AF relay is re-transmitted to the destination using an amplifying factor. The output SNR signal information is given by;

$$\mathscr{Y}_{r_1,d} = \sqrt{\mathscr{P}_{r_1}} h_{r_1,d} \mathscr{Y}_{s,r_1} + \mathscr{Z}_{r_1,d} \tag{4}$$

where, $h_{r_1,d}$ is the channel gain of the relay to the destination, $\mathscr{Y}_{s,r_1}$ are the transmitted signals from $S \rightarrow R$, and $\mathscr{Z}_{r_1,d}$ is the zero-mean AWGN, with unit variance at the destination.

By substituting Eq. (3) into (4) to obtain amplified signal information at the destination from the source and through the relay device. The output SNR expression is given as;

$$y_{r_1,d} = \frac{\sqrt{p}}{\sqrt{p\left|h_{s,r}\right|^2 + 1}} \sqrt{p_{r_1}} h_{r_1,d} * y_{s,r_1} + Z_{r_1,d} \tag{5}$$

where, $h_{s,r}$ is the channel gain ($S \rightarrow R$), $h_{r_1,d}$ is the channel gain ($R \rightarrow D$), $\mathscr{P}_{r_1}$ is the symbol power ($R \rightarrow D$).

By substituting Eq. (1) into (5), the output SNR $\left(\mathscr{Y}_{r_1,d(AF)}\right)$ from AF relay to the destination is expressed as;

$$\mathscr{Y}_{r_1,d(AF)} = \mathscr{K}_r{}^{(AF)} \sqrt{\mathscr{P}_{r_1}} h_{r_1,d} * \left(\sqrt{\mathscr{P}_s}\, h_{s,r_1}\, \mathscr{X}_\tau + \mathscr{Z}_{s,r_1}\right) + \mathscr{Z}_{r_1,d} \tag{6}$$

$$\mathscr{Y}_{r_1,d(AF)} = \mathscr{K}_r{}^{(AF)} \sqrt{\mathscr{P}_s \mathscr{P}_{r_1}}\, h_{s,r_1} h_{r_1,d}\, \mathscr{X}_\tau + \mathscr{K}_r{}^{(AF)} \sqrt{\mathscr{P}_{r_1}} h_{r_1,d} \mathscr{Z}_{s_1,r} + \mathscr{Z}_{r_1,d} \tag{7}$$

The term $\mathscr{Z}_{s,r_1}$ in Eq. (7) is the channel noise is modelled as zero-mean independent AWGN, with unit variance at the relay and destination. Here, the noise $Z \sim \mathscr{N}(0, \mathscr{N})$ is a Gaussian random variable with zero (0) mean and variance $\mathscr{N}$. It is a standard practice to introduce a shorthand notation to describe a Gaussian random variable, where $Z = 0$ and variance $\mathscr{N}$ has a unit value.

$$\mathscr{Y}_{r_1,d(AF)} = \mathscr{K}_r{}^{(AF)} \sqrt{\mathscr{P}_s \mathscr{P}_{r_1}}\, h_{s,r_1} h_{r_1,d}\, \mathscr{X}_\tau + \mathscr{Z}_{r_1,d} \tag{8}$$

It should be noted that two copies of the signal $\mathscr{X}_\tau$ both from the source link and the relay protocol device are received at the destination. The joint optimisation combiner transmitted symbols to the destination depending on the number of relay devices in the system.

3.4. Decode-forward (DF) relay protocol

In DF phase 1, the source broadcasts the symbol information directly through the relay device based on Eq. (1), and to the destination node using Eq. (2). The signal information $\mathscr{Y}_{s,\,r_1}$ is received at the DF relay device, while $\mathscr{Y}_{s,d}$ is received from the source at the destination. In DF phase 2, the DF relay decodes the signal, re-encodes it, and forwards the information with power $\mathscr{P}_{r_1}$ to the destination. In this case, the DF relay can only decode the source signal when the SNR of the source signal exceeds, or equal the threshold value; otherwise, the relay remains silent or dormant. If the DF relay decodes source signal correctly based on the predefined threshold, then, $\mathscr{P}_s = \mathscr{P}_{r_1}$, otherwise $\mathscr{P}_{r_1} = 0$. The output SNR at the destination without amplification factor in DF phase 2 is expressed in [39] as;

$$\mathscr{Y}_{r_1,d(DF)} = \sqrt{\mathscr{P}_{r_1}} h_{r_1,\,d} * \mathscr{Y}_{s,\,r_1} + \mathscr{Z}_{r_1,d} \tag{9}$$

where, $\mathscr{Y}_{r_1,d(DF)}$ is the output SNR, $h_{r,d}$ is the channel gain from $R \rightarrow D$, $\mathscr{Y}_{s,r}$ is the transmitted symbol from $S \rightarrow R$ and $\mathscr{Z}_{r_1,d}$ is the zero-mean independent AWGN, with unit variance at the relay and destination.

Therefore, substituting $\mathscr{Y}_{s,\,r_1}$, in Eq. (1) into (9) and expanding to obtain the output instantaneous SNR at the destination through

the DF relay device yields;

$$\mathscr{Y}_{r_1,d(DF)} = \sqrt{\mathscr{P}_{r_1}} h_{r_1,\ d} * \left(\sqrt{\mathscr{P}_s}\ h_{s,\ r_1}\ \mathscr{X}_\tau + \mathscr{Z}_{s,r_1}\right) + \mathscr{Z}_{r_1,d} \tag{10}$$

$$\mathscr{Y}_{r_1,d(DF)} = \sqrt{\mathscr{P}_s \mathscr{P}_{r_1}} h_{s,\ r_1} h_{r_1,\ d} * \mathscr{X}_\tau + \sqrt{\mathscr{P}_{r_1}} h_{r_1,\ d} * \mathscr{Z}_{s,r_1} + \mathscr{Z}_{r_1,d} \tag{11}$$

where, $\mathscr{Z}_{s,r_1}$ is the channel noise, modelled as the zero-mean independent AWGN, with unit variance at the relay and destination. Some other channel noise will be absorbed with the deployment of the matched filter at the diversity stage in the receiver. Therefore, the noise due to channel impairment is assumed to be zero, and Eq. (11) becomes.

$$\mathscr{Y}_{r_1,d(DF)} = \sqrt{\mathscr{P}_s \mathscr{P}_{r_1}} h_{s,r} h_{r,d} * \mathscr{X}_\tau + \mathscr{Z}_{r_1,d} \tag{12}$$

The signal $(\mathscr{X}_\tau)$ from the source and relay devices are received at the destination. The MRC technique combines copies of the transmitted symbols at the destination, depending on the number of relay devices in the system.

3.5. IoF hybrid amplify and decode forward (HADF) protocol

As depicted in Fig. 1, the IoT-Fog HADF protocol is a hybrid cooperative relay system comprising the source, relay device, and destination sink. This new hybrid relay protocol combines AF and DF protocols to ensure better and more reliable signal transmission at the destination. In HADF phase 1, the source broadcasts symbol information to both the hybrid device and the destination. Eqs. (1) and (2) represent the transmitted symbols $\mathscr{Y}_{s,\ r_1}$ and $\mathscr{Y}_{s,d}$ from the source to the hybrid HADF relay device, and from the source to the destination, respectively. In HADF phase 2, the hybrid relay device, which consists of an AF and DF relay, either amplifies- Forward or the Decode-Forward, the received symbol to the destination. The new hybrid relay was achieved with the combination of Eqs. (8) and (12) to obtain the transmitted symbol from hybrid relay 1 to the destination. The output SNR of hybrid relay 1 is denoted as $y_{r_1,\ d(H)}$, at the destination is given by Eq. (13).

$$\mathscr{Y}_{r_1,\ d(H)} = \mathscr{K}_r{}^{(AF)} \sqrt{\mathscr{P}_s \mathscr{P}_{r_1}} h_{s,r_1} h_{r_1,\ d} * \mathscr{X}_\tau + \mathscr{Z}_{r_1,d} + \left(\mathscr{Y}_{r_1,d(DF)}\right) \tag{13}$$

$$\mathscr{Y}_{r_1,\ d(H)} = \left[\mathscr{K}_r{}^{(AF)} \sqrt{\mathscr{P}_s \mathscr{P}_{r_1}}\ h_{s,r_1} h_{r_1,\ d} * \mathscr{X}_\tau + \mathscr{Z}_{r_1,d} + \left(\sqrt{\mathscr{P}_s \mathscr{P}_{r_1}}\ h_{s,r_1} h_{r_1,\ d} * \mathscr{X}_\tau + \mathscr{Z}_{r_1,d}\right)\right] \tag{14}$$

$$\mathscr{Y}_{r_1,\ d(H)} = \left[\sqrt{\mathscr{P}_s \mathscr{P}_{r_1}}\ h_{s,r_1} \left(\mathscr{K}_r{}^{(AF)} h_{r_1,\ d} * \mathscr{X}_{\tau(AF)} + h_{r_1,d} * \mathscr{X}_{\tau(DF)}\right)\right] \tag{15}$$

where, $\mathscr{Y}_{r_1,\ d(H)}$ is the output SNR of the hybrid at relay 1, $\mathscr{K}_r{}^{(AF)}$ is the AF protocol amplification factor, P_s is the signal power at the source, $\mathscr{P}_{r_1}$ is the hybrid signal power, $P = P_s = \mathscr{P}_{r_1}$, $h_{s,r}$ and $h_{s,d}$ are the channel gain or channel coefficient, and $\mathscr{X}_\tau$ is the transmitted symbol. The equivalent hybrid independent noise $\mathscr{Z}_{r_1,d}$ is the channel noise modelled as zero (0) mean AWGN with unit variance $\mathscr{N}$, where $Z = 0$ and variance $\mathscr{N}$ has a unit value. The MF was deployed to filter out the remaining noisy signal. The first HADF device is expected to forward the information symbol to both relay 2 and the destination. The received symbol from HADF relay 1 to 2 is essential. Therefore, the output of the hybrid relay 1 to 2 $\left(\mathscr{Y}_{r_1,\ r_2(H)}\right)$ is given by;

$$\mathscr{Y}_{r_1,\ r_2(H)} = \left[\sqrt{\mathscr{P}_s \mathscr{P}_{r_1}}\ \left(\mathscr{K}_r{}^{(AF)} h_{r_1,\ r_2,} * \mathscr{X}_{\tau(AF)} + h_{r_1,\ r_2,} * \mathscr{X}_{\tau(DF)}\right)\right] \tag{16}$$

where, $h_{r_1,\ r_2,}$ is the channel coefficient from relay 1 to relay 2, and $\mathscr{Y}_{r_1,\ r_2(H)}$ is the output SNR

The information symbol from hybrid relay 2 is also transmitted to the destination node. The output SNR is expressed in Eq. (17) as;

$$\mathscr{Y}_{r_2,\ d(H)} = \left[\sqrt{\mathscr{P}_s \mathscr{P}_{r_1}}\ h_{r_1,\ r_2,}\ \left(\mathscr{K}_r{}^{(AF)} h_{r_2,\ d} * \mathscr{X}_{\tau(AF)} + h_{r_2,\ d} * \mathscr{X}_{\tau(DF)}\right)\right] \tag{17}$$

where, $\mathscr{Y}_{r_2,\ d(H)}$ is the output SNR, and $h_{r_2,\ d}$ is the channel coefficient from relay 2 directly to the destination.

Furthermore, the second HADF device will forward the information symbol to relay 3 and the destination node. The received information symbol from HADF relay 1 to 2 is also relevant. Therefore, the output SNR of the hybrid relay 2 to 3 $\left(\mathscr{Y}_{r_2,\ r_3(H)}\right)$ is presented as;

$$\mathscr{Y}_{r_2,\ r_3(H)} = \left[\sqrt{\mathscr{P}_s \mathscr{P}_{r_2}}\ \left(\mathscr{K}_r{}^{(AF)} h_{r_2,\ r_3,} * \mathscr{X}_{\tau(AF)} + h_{r_2,\ r_3,} * \mathscr{X}_{\tau(DF)}\right)\right] \tag{18}$$

where, $h_{r_2,\ r_3,}$ is the channel coefficient from relay 2 to relay 3, and $\mathscr{Y}_{r_2,\ r_3(H)}$ is the output SNR

The information symbol from hybrid relay 3 is also transmitted to the destination node. The output SNR is expressed in Eq. (19) as;

$$\mathscr{Y}_{r_3,\ d(H)} = \left[\sqrt{\mathscr{P}_s \mathscr{P}_{r_1}}\ h_{r_2,\ r_3,}\ \left(\mathscr{K}_r{}^{(AF)} h_{r_3,\ d} * \mathscr{X}_{\tau(AF)} + h_{r_3,\ d} * \mathscr{X}_{\tau(DF)}\right)\right] \tag{19}$$

where, $\mathscr{Y}_{r_3,\ d(H)}$ is the output SNR, and $h_{r_3,\ d}$ is the channel coefficient from relay 3 directly to the destination.

The condition of the relay device switching of the new HADF model depends on the activated network operations. The hybrid relay must fulfil the system model condition in terms of signal level and predefined threshold to achieve better network performance.

Finally, the JOC maps and forwards the transmitted symbols from the source, hybrid relay 1, and hybrid relay 2 to the destination sink in Fig. 2.

Appendix A (Algorithm I) provides a systematic, step-by-step protocol for the IoT-HADF system while optimising network performance under challenging channel conditions. From Fig. 2a, the overall output SNR obtained at the destination sink is given as.

$$\mathscr{Y}_{d(MRC)\ [H]} = \frac{1}{n}\left(\sum_{i=1}^{k} \mathscr{Y}_{i,d}\right) \tag{20}$$

where, $\mathscr{Y}_{d(MRC)\ [H]}$ is the output SNR at the destination receiver, and $\mathscr{Y}_{i,d}$ is the output SNR of each carrier for the fading process $i = 1, 2 \ldots k$. The MRC detector with Matched Filter (MF) adds all the signal paths and sends out the average as the output to the user at the destination. The MRC simplified expression for the combined signal at the destination is given as;

$$y_{d(MRC)}\ [n] = \frac{1}{n}\left(\sum_{i=1}^{k} \mathscr{Y}_{s,d} + \mathscr{Y}_{r_1,\ d(H)} + \mathscr{Y}_{r_2,\ d(H)} + \mathscr{Y}_{r_3,\ d(H)}\right) \tag{21}$$

The simulation was carried out using MATLAB 2022b software to compare existing relays, such as AF and DF with the HADF hybridized model. The parameters employed was presented in Table 2.

3.6. Nakagami-m fading and path loss model

The wireless channels in the HDAF framework are modelled using Nakagami-*m* fading to capture multipath effects commonly observed in industrial IoT–Fog environments. The m-parameter represents fading severity:

- $m > 1$for line-of-sight (LOS) dominant links
- $0.5 \leq m < 1$for non-line-of-sight (NLOS) or heavily obstructed links [40].

In our MATLAB simulations and TelosB testbed experiments, we use $m = 2$, representing mild fading with partial LOS, which is typical for semi-obstructed industrial indoor environments. This choice is supported by the testbed observations and ensures realistic evaluation of protocol performance.

Path loss is modelled using the log-distance model [41,42]:

$$PL(d) = PL(d_0) + 10n\log_{10}\frac{d}{d_0} + X_\sigma \tag{22}$$

where:$PL(d_0)$is the reference path loss at distance d_0, $n$is the path-loss exponent, $X_\sigma$is zero-mean Gaussian shadowing in dB.

For our evaluation (Section 5.3), we consider a semi-obstructed industrial indoor environment typical of IoT–Fog deployments. The simulation and testbed setups are configured to reflect realistic industrial conditions, including moderate signal attenuation and variable obstruction levels, ensuring that performance metrics such as BER, latency, and coverage provide an accurate assessment of HDAF under practical deployment scenarios.

4. System algorithm design

While the HDAF concept itself is established, the novelty of this work lies in its integration within a fog relay architecture and the use of a software-defined control interface for real-time analytics (i.e., SIF-IRN). The relay switching mechanism is adaptive, based on the instantaneous SNR measured at each relay. We designed Algorithm 1 (Appendix 1) to enable the cooperative edge-to-sink system to

Fig. 2a. IoT–Fog experimental data collected using the IoF-HDAF protocol for environmental monitoring of pipeline ambient conditions at SPDC's CCP/CPF gas plant, North Bank, Delta State, Nigeria.

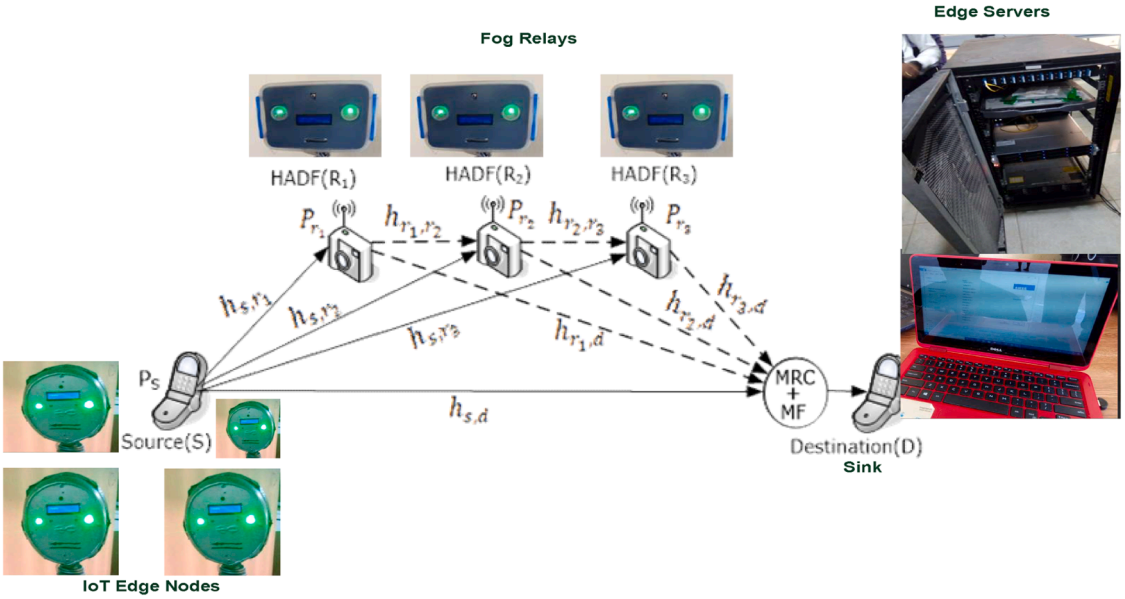

Fig. 2b. IoT–Fog robot multi-node cooperative repeater model. The edge-detecting agent employs Algorithm I to implement a systematic, step-by-step protocol for the IoT-Fog HADF framework, optimising network performance under challenging channel conditions. This experimental IoT-Fog use case illustrates IoF-HDAF nodes deployed for pipeline monitoring applications.

Table 2
Physical-layer simulation parameters. Summary of all configurable parameters used in MATLAB simulations and real-world testbed experiments.

Parameter	Variable
Modulation	QPSK, Offset- QPSK (OQPSK in 802.15.4)
Frequency	2.4 GHz
Number of symbols	20,000
SNR	0–10 dB
Transmit power $P = P_1 = P_2$	0 dBm (1 mW)
Packet duration	4–10 ms (802.15.4 frame)
HDAF threshold	5 dB
Bandwidth	2 MHz (IEEE 802.15.4 channel)

operate with three hybrid relay protocols. The HDAF protocol efficiently decodes, amplifies, and forwards the source signal to the destination combiner. In this system, the AF or DF relay mode may either remain silent or transmit information symbols depending on the quality of the signal received by the HDAF relay. Specifically, when the transmitted signal falls below a predefined threshold and cannot be correctly decoded by the DF relay, the DF relay remains dormant while the AF relay amplifies and forwards the signal to the destination combiner. At the destination, a JOC technique enhanced with a matched filter aggregates the transmitted symbols. The JOC combines only signals that meet the predefined threshold criteria and averages the contributions from all active relay paths. The resulting average instantaneous SNR, obtained via MRC, is delivered to the user. The output SNR of the optimisation combiner follows a Nakagami fading channel model. A three-node cooperative relaying scenario is illustrated in Figs. 2(a)–(c), where the receiver mitigates fading by coherently adding the contributions of all relay signals. Section 7 presents simulation results and experimental measurements demonstrating the protocol's superiority over conventional relaying schemes (AF, DF, and selective wireless relaying, SWR) in terms of BER and CC. The underlying relay mechanisms are discussed in detail in Section 4.1.

4.1. Description of HDAF relay mechanism

The HDAF relay mechanism is an adaptive relaying protocol designed to overcome the individual shortcomings of conventional DF and AF schemes (See below).

i. Decision rule: If $\mathscr{Y}_{s,r_1} \geq \gamma_{th}$ DF is used, eliminating first-hop noise and decode the received signal into bits. Then, perform cyclic redundancy check (CRC) error detection. The CRC or error-detection codes verify decoded bits; if successful, re-encode, modulate, and forward. If CRC fails, fall back to AF to avoid forwarding wrong bits. where, γ_{th} is the threshold chosen empirically to minimise

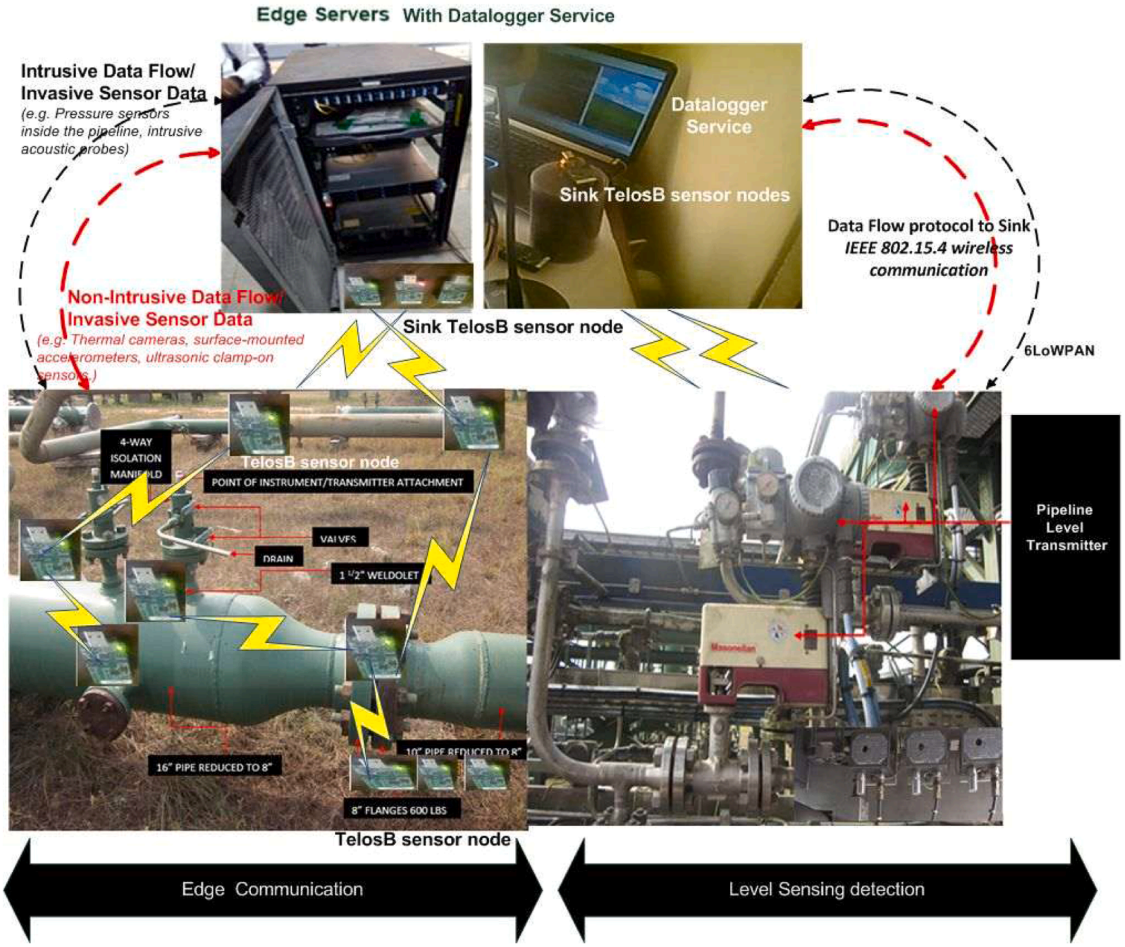

Fig. 2c. Installed on AG Compressor Train B at SPDC's CCP/CPF gas plant (Northbank): a Smart Sensor System S104 combustible-gas detector; single and dual level transmitters; and three Rosemount 3051/3001 pressure transmitters—each fitted with Fieldbus communication cables, with the level transmitters also supporting HART. This setup was replaced with TelosB sensor nodes for data acquisition.

BER and maximise Channel Capacity. If $\mathscr{Y}_{s,r_1} < \gamma_{th}$. AF is used with controlled gain and noise filtering to limit noise amplification using Eq. (3), before forwarding.

ii. SNR Measurement at the Relay

The relay estimates noise variance N_0 and received signal power $\mathscr{P}_{r_x}$, then computes $SNR = \mathscr{P}_{r_x}/N_0$. This ensures AF is only used when DF decoding is not reliable.

iii. Destination Signal Combining

The destination uses maximal ratio combining (MRC) to merge the direct source–destination link and–relay-destination signal (processed by DF or AF). Finally, MRC down-weights the noisy AF signal if its SNR is poor and applies a matched filter to AF noisy paths, reducing noise impact. This ensures AF noise does not dominate the combined decision

iv. Adaptive Decision

In HDAF, the selection criteria are adaptive to the fact that the relay measures the instantaneous SNR, $\mathscr{Y}_{s,r}$ in *real time* for every transmission block. Based on this measured SNR compared to the threshold γ_{th}, the relay decides dynamically whether to use DF or AF. It is Adaptive because the relay evaluates the channel SNR each time and switches mode accordingly.

In Section 4, we propose a novel HDAF relay protocol to improve reliability, coverage, and energy efficiency in IoT–Fog networks. The protocol adaptively selects between DF and AF at each relay based on real-time channel conditions, and its performance is validated through MATLAB simulations and a real-world testbed. Key contributions include the design of an intent-driven adaptive relay mechanism for signal management. In Section 5, we considered the experimental demonstration in industrial IoT environments and integration with heterogeneous IoT–5G networks. In Section 6, the results demonstrated significant improvements in link reliability, latency, throughput, and energy efficiency compared with traditional relay schemes.

5. IoT-Fog experimental use case

We have developed the analytical model and validated the proposed HDAF protocol through experimental and numerical simulation. This was done under Nakagami-*m* fading to demonstrate applicability in real-world IoT–Fog environments. Field experiments were conducted using 2.4 GHz IEEE 802.15.4/Zigbee-compliant TelosB motes equipped with CC2420 transceivers, MSP430 microcontrollers, and modular sensor arrays, enabling real-time environmental monitoring and adaptive relay operation.

5.1. Real world setup

IoT–Fog HDAF protocol was validated at Shell Petroleum Development Company's (SPDC) Central Control Plant/Central Processing Facility (NorthBank, Delta State, Nigeria), monitoring pipeline ambient conditions. The testbed consisted of TelosB motes with CC2420 transceivers (2.4–2.4835 GHz, 250 kbps), MSP430 microcontrollers running TinyOS, and modular sensor arrays measuring temperature, humidity, and light. Two deployment configurations were used: (i) an outdoor setup around the compressor train with a laptop-connected sink node and three peripheral nodes positioned at 0°, 90°, and 180° offsets, and (ii) a mirrored indoor setup along the control-building corridor. Nodes sampled and transmitted environmental data every 5 seconds via the IoT–Fog HDAF protocol, routing data intelligently through edge and Fog relays to the sink (See Fig. 2c).

Central to the deployment, the Software-Defined Coupling (SDC) module implements intent-based control, dynamically adjusting relay modes, transmission power, and routing paths based on real-time link quality, interference, and SNR (See Fig. 2d). This ensures the network achieves its objectives of maximising signal integrity, mitigating interference, and maintaining reliable, low-latency communication. Averaged measurements across both indoor and outdoor setups provided a robust evaluation of the protocol's performance. While the experimental validation uses 2.4 GHz Zigbee, the analytical and simulation model targets 3.5 GHz 5G NR. Integration between Zigbee and 5G is achieved via dual-radio IoT–Fog gateways performing protocol translation, traffic aggregation, and QoS mapping. The HDAF protocol operates above the PHY layer at the gateway/fog level, rendering relay selection, interference mitigation, and forwarding logic independent of the access-network carrier frequency, with frequency-specific effects captured through parameterised propagation models. This design choice demonstrates the practical applicability of HDAF in heterogeneous IIoT–5G networks, effectively bridging low-power local IoT links with high-reliability 5G backhaul connectivity.

5.2. Real-world validation and algorithm implementation

5.2.1. The intent-based HDAF relay selection algorithm

Fig. 2e was implemented to manage relay selection in the field. Inputs included the number of IoT sensor nodes (N_p), cooperative Fog relays (N_c), channel state information (CSI) including instantaneous SNR per link, and high-level service intents $I = \{R, L, T\}$ specifying reliability, latency, and throughput requirements.

Forwarding Schedules (SF slots 7–12) were assigned to each relay cluster as discrete timeslots to coordinate packet forwarding, avoid collisions, and mitigate interference. Note that SF slots 7–12 were selected to align with the contention-free region of the IEEE 802.15.4 superframe. It provides sufficient time for channel estimation, AF/DF mode selection, and intent-aware scheduling while

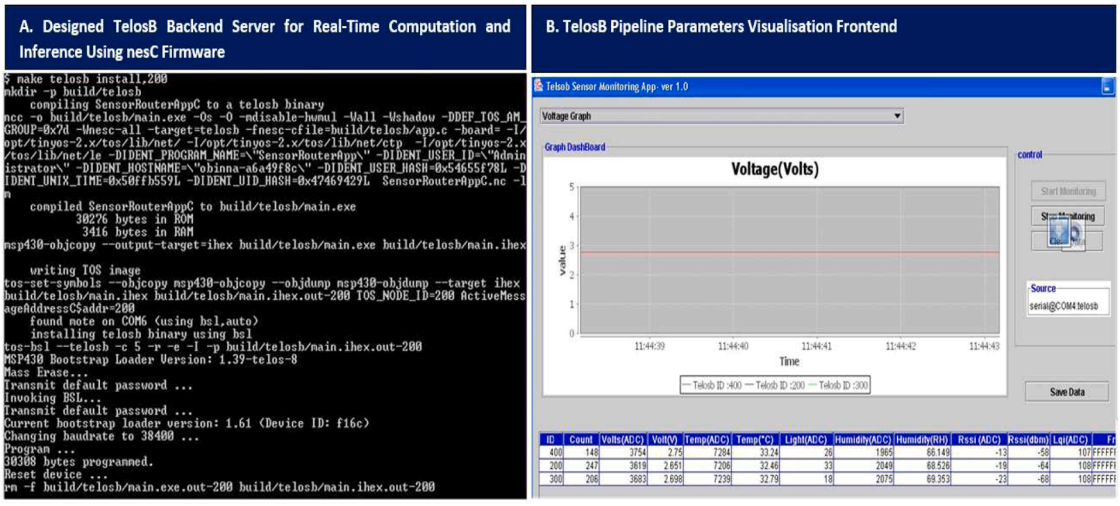

Fig. 2d. TelosB intent-based datalogger backend and web interface, where edge and fog relay nodes are integrated via Software-Defined Coupling (SDC) agent. The system provides scalable orchestration and efficient real-time data processing within the IoT–Fog HDAF framework. It supports continuous acquisition of pressure, level, and gas-concentration streams over IEEE 802.15.4 from pipeline sensors. Edge signal-conditioning and timestamp-alignment modules synchronise and preprocess raw data before backend storage in time-series format. The interactive dashboard visualises live telemetry, analytics metrics, and configurable alert thresholds.

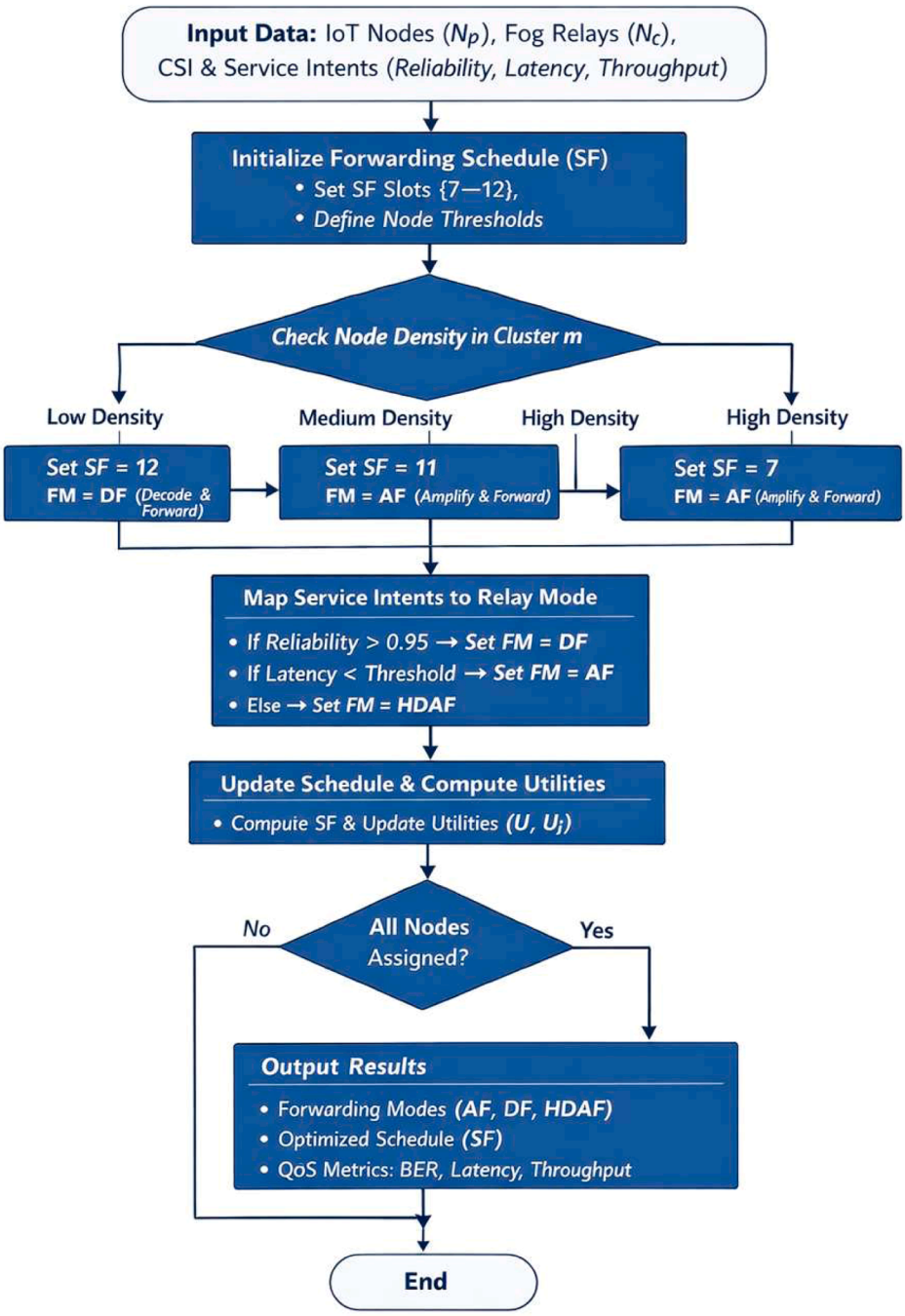

Fig. 2e. Intent-based HDAF relay selection flowchart algorithm and forwarding schedule (SF slots 7–12) implementation in IoT–Fog–5G field experiments at SPDC CCP/CPF gas plant.

minimising contention and interference in dense IoT–Fog relay clusters. Each SF slot defines when and how a relay transmits and is dynamically adjusted based on node density, channel conditions, and service intents to optimise latency, reliability, and throughput in conjunction with hybrid AF/DF relaying.

Clusters were processed iteratively: nodes with high reliability requirements adopted DF, latency-sensitive nodes used AF, and hybrid HDAF mode balanced both objectives. Service intents were mapped to relay decisions for adaptive mode selection, while forwarding schedules and cooperative utility functions were updated iteratively until all nodes were allocated. The algorithm outputs optimised relay modes ($FM = \{AF, DF\}$), SF allocations for each relay cluster, and enhanced QoS metrics including bit error rate (BER),

latency, and throughput demonstrating a scalable, AI–Fog-driven, interference-resilient communication framework. During the SPDC field experiment, SF slots 7–12 effectively coordinated packet forwarding among Fog relay clusters, enabling the IoT–Fog HDAF protocol to adapt frame size, relay mode, and forwarding schedules in real time. Environmental and network metrics from TelosB nodes, including voltage, temperature, humidity, RSSI, and frame size, confirmed that SF-enabled relay coordination efficiently managed interference, preserved packet order, and maximised throughput. Stronger RSSI values were associated with larger frames, increasing throughput, while weaker signals corresponded to smaller frames, reducing effective throughput; this highlights the adaptive behaviour of the protocol in managing transmission efficiency. Table 3 summarises the environmental and network metrics recorded by Node 301. Voltage remained stable (2.780–2.783 V), temperature ranged from 30.82 to 31.38 °C, and relative humidity varied slightly (62.215–64.285%). RSSI fluctuated between –43 dBm and –37 dBm, influencing frame sizes from 2 to 8 bytes.

In all these, the experiments conducted in outdoor compressor train areas and indoor corridors captured mobility-induced variations and multipath effects, with mobile nodes displaced up to 100 m. Node 302, for example, exhibited RSSI fluctuations of –60 dBm to –74 dBm during indoor–outdoor transitions, whereas Nodes 301 and 303 maintained voltage stability (~2.77–2.81 V) and accurate environmental sensing. The "Count" column in Table 3 represents sequential packet numbers for traceability, enabling detection of dropped or out-of-order packets and preserving the integrity of the time-series data. Voltage readings remained stable, confirming minimal power fluctuation. Temperature and humidity showed minor variation, indicating stable ambient conditions. In contrast, RSSI variations directly influenced frame size and throughput, with stronger RSSI values enabling larger frames (6–8) and higher effective data rates, and weaker RSSI yielding smaller frames (2–3) and lower throughput. In context, the testbed was deliberately designed to capture mobility and interference variability. IoT mobile nodes (IDs 301, 302, 303) were displaced up to 100 m in controlled mobility trials to validate protocol robustness. The dual deployment environments (i) outdoor compressor train areas with metallic structures, RF reflections, and fluctuating interference, and (ii) indoor control-building corridors with multipath and attenuation enabled realistic stress-testing of link reliability, throughput, and latency. While single-hop edge-to-fog communication was the primary focus, multi-hop dynamics were implicitly enabled through the Software-Defined Coupling (SDC) mechanism, adaptively balancing traffic between edge and Fog relays while maintaining interference mitigation, packet integrity, and reliability. The datasets recorded during mobility experiments in Appendix B illustrate robustness. For instance, Node 302 experienced RSSI fluctuations from –60 dBm to –74 dBm, whereas Nodes 301 and 303 maintained voltage stability and consistent environmental sensing over displacements up to 100 m. These results demonstrate the protocol's resilience to interference, mobility, and channel variability.

Throughput remained maximised under dynamic SF slot coordination and hybrid relay selection, ensuring efficient frame delivery even under fluctuating RSSI and node density.

5.2.2. Algorithm scalability and complexity analysis

The relay selection and SF allocation algorithm iteratively processes each Fog cluster and evaluates node density and channel conditions. Each decision requires only simple arithmetic comparisons and threshold checks per node, without computationally intensive operations. This low-complexity, rule-based approach ensures real-time applicability in industrial IoT–Fog deployments, capturing the core behaviour of AI-Fog decision-making (intent-driven, adaptive relay selection) while remaining practical for large-scale networks. Overall, the combination of SF slot assignment, hybrid AF/DF relay selection, and SDC-enabled adaptive forwarding ensured interference-resilient, low-latency, and high-throughput communication. These results, corroborated by simulations under Nakagami-m fading, confirm the practical effectiveness of the IoT–Fog HDAF protocol in bridging low-power IoT networks with 5G infrastructure, delivering robust QoS under variable environmental, mobility, and multi-hop conditions. Extension to controlled multi-hop chains is identified as a direction for future work to further strengthen throughput and latency analysis.

5.3. Simulation and experimental validation

5.3.1. Experimental setup and parameter configuration

To ensure consistency across the analytical modelling, MATLAB simulations, and the TelosB testbed, all physical-layer, channel, and network-layer parameters were harmonised, as summarised in Table 4. A random waypoint mobility model with node speeds of 0–3 m/s emulates mobile sensors and Fog relays in industrial IoT environments. The system employs a multi-hop IoT–Fog relay topology, where intermediate nodes enhance coverage and reliability. Wireless links were modelled using Nakagami-m fading ($m = 2$)

Table 3
Environmental and network metrics recorded by TelosB node 301 during the IoF-HDAF field experiment at SPDC's CCP/CPF gas plant.

S/ No	Telsob ID	Count	Voltage (V)	Temperature (°C)	Humidity (RH)	Rssi(dbm)	Frame size
1	301	179	2.783	30.82	62.659	-43	2
2	301	180	2.780	**30.87**	63.185	-39	6
3	301	181	2.783	30.99	64.115	-41	4
4	301	182	2.781	31.10	64.285	-42	3
5	301	183	2.781	31.12	63.408	-42	3
6	301	184	2.780	31.28	63.160	-37	8
7	301	185	2.782	31.38	63.145	-42	3
8	301	186	2.780	31.35	63.293	-39	6
9	301	187	2.782	31.11	62.215	-41	4
10	301	188	2.780	31.13	63.410	-41	4

and a path-loss exponent $n = 2.2$ [40,41]. This is calibrated via RSSI measurements to match the experimental deployment in Section 5.2. Packet loss was quantified through cyclic redundancy check (CRC) failures and acknowledgement (ACK) timeouts in the testbed and derived from BER in MATLAB. End-to-end latency incorporates relay processing, queuing, retransmissions, and propagation delays, consistently defined across both simulation and experimental environments. Cross-layer validation, including BER versus SNR, throughput versus relay distance, RSSI, packet delivery ratio (PDR), and latency, demonstrated strong agreement between MATLAB simulations and testbed observations, confirming the accuracy and physical relevance of the models. Together with baseline industrial metrics (Table 5), these results demonstrate that the HDAF framework is both theoretically sound and practically implementable in industrial wireless networks.

5.4. Protocol validation and benchmarking

For protocol validation, identical parameters were applied in both MATLAB simulations and the TelosB testbed. Performance was evaluated relative to a baseline scenario without HDAF, using standard industrial metrics such as packet delay and BER. This baseline enables quantification of the HDAF protocol's hybrid dual-antenna mechanism, interference mitigation, and adaptive forwarding gains. Cross-layer validation confirmed that MATLAB simulations closely replicate real-world experimental conditions, including transmit power, noise floor, data rate, fading environment, and mobility patterns. The results demonstrate that the HDAF framework is scalable, robust, and suitable for practical industrial IoT deployments.

5.5. Practical applications of IoT–Fog HDAF

The IoT–Fog HDAF communication framework is well-suited for industrial environments requiring reliable and low-latency communication. Typical application scenarios include factory-floor monitoring, refinery and pipeline inspection, smart manufacturing systems, and mobile maintenance operations [43–45]. The hybrid AF–DF relaying strategy dynamically selects the optimal forwarding mode based on instantaneous channel conditions, reducing packet loss and latency. By leveraging nearby Fog gateways, the system enables local decision-making and continued operation during backhaul disruptions. TelosB-based testbed experiments confirm that these benefits are achievable on resource-constrained industrial hardware, demonstrating practical applicability beyond laboratory environments.

5.6. Channel capacity and latency analysis

In wireless, 5G, IIoT, and industrial networks, limited bandwidth and interference reduce SNR, which in turn reduces channel capacity, leading to: Lower throughput, Higher delay (latency), Higher packet loss and retransmissions. This is why interference mitigation and cooperative relaying (e.g., HDAF protocol) are critical: they increase effective SNR, thereby increasing channel capacity and reliability. Channel capacity (C_{HDAF}) is the highest achievable bit rate (bits/*sec*) at which data can be sent reliably over a communication channel, given its bandwidth and noise level. The achievable CC of the HDAF is computed using the Shannon–Hartley theorem:

$$C_{\mathrm{HDAF}} = B \cdot \log_2(1+\gamma_{\mathrm{HDAF}}), \gamma_{\mathrm{HDAF}} = \max\left(\gamma_{\mathrm{AF}}, \gamma_{\mathrm{DF}}\right) \tag{23}$$

where B is the system bandwidth (Hz) and $\gamma_{\mathrm{AF}}$and γ_{DF} are the instantenous received SNRs for the AF and DF paths, respectively. The HDAF hybrid scheme selects the path with the higher instantaneous SNR, maximising throughput under varying channel conditions.

Latency/End-to-end latency (T_{E2E}) is the total time taken for a data packet to travel through the network, including transmission, propagation, processing, and queuing delays. The end-to-end latency $T_{\mathrm{E2E}}$is defined as Eq. (24):

$$T_{\mathrm{E2E}} = T_{\mathrm{tx}} + T_{\mathrm{relay}} + T_{\mathrm{queue}} + T_{\mathrm{prop}} \tag{24}$$

where T_{tx}= transmission time of a packet, T_{relay}= processing delay at the relay node, T_{queue}= queuing and scheduling delays, T_{prop}= propagation delay. Mean latency ($\bar{T}_{\mathrm{E2E}}$) is given by Eq. (25):

Table 4
Comparison of MATLAB simulation and TelosB testbed parameters.

Parameter	MATLAB simulation	TelosB testbed
Carrier frequency	2.4 GHz	2.4 GHz
Standard	IEEE 802.15.4	IEEE 802.15.4 (CC2420)
Data rate	250 kbps	250 kbps
Transmit power	0 dBm	0 dBm
Noise floor	−100 dBm	−100 dBm (measured)
Packet size	64 bytes	64 bytes
Relay spacing	10–50 m	10–50 m
Path-loss exponent	$n = 2.2$	Fitted from RSSI
Fading model	Nakagami-m ($m = 2$)	Industrial indoor fading
Mobility speed	0–3 m/s	Human/device movement

Table 5
Baseline real-world performance metrics for Industrial IoT CPS. This shows the typical, and required performance values in real industrial IoT / CPS networks.

Metric	Real-world values
Zigbee / Fieldbus data rate	250 kbps
Typical industrial packet delay	100 to 500 ms
BER without relays in interference	10^{-2} to 10^{-3}
Required BER for industrial CPS	10^{-5} or better
Required latency	$<$ 10–20 ms

$$\bar{T}_{\mathrm{E2E}} = \frac{1}{N}\sum_{i=1}^{N} T_{\mathrm{E2E}}^{(i)} \tag{25}$$

Both MATLAB simulations and TelosB testbed experiments were used to measure T_{E2E}. Each scenario was repeated multiple times (over 30 independent runs) to compute the mean and standard deviation, capturing variability due to fading, mobility, and environmental interference. Example results (mean ± std) show HDAF achieves lower latency than conventional AF and DF protocols. Table 6 shows end-to-end latency results (mean ± standard deviation) for different relaying protocols.

5.7. Statistical significance and confidence interval analysis

The statistical significance of the end-to-end latency results was evaluated using 95% confidence intervals (CI) computed over 30 independent runs. Table 7 summarises the mean latency, standard deviation, and the associated confidence-interval parameters for each protocol. End-to-End Latency CI Parameters for formula is given as: [42]

$$\mathrm{CI}_{95\%}^{\mathrm{latency}} = \bar{T}_{\mathrm{E2E}} \pm 1.96 \cdot \frac{\sigma_{\mathrm{latency}}}{\sqrt{N}} \tag{26}$$

Definitions of parameters: $\bar{T}_{\mathrm{E2E}}$ = mean latency measured over 30 repeated runs (ms), $\sigma_{\mathrm{latency}}$ = standard deviation of latency over 30 runs (ms), $N = 30$ simulation/testbed runs, SE = $\sigma_{\mathrm{latency}}/\sqrt{N}$ = standard error, 1.96 = Z-score for 95% confidence, and 95% CI = $\bar{T}_{\mathrm{E2E}} \pm 1.96 \cdot SE$

To assess the statistical reliability of the bit-error rate (BER) results, the mean BER and 95% confidence intervals were computed based on repeated transmissions over $N_{\mathrm{bits}} = 10^6$bits per run (for 30 independent runs). The parameters used to derive these confidence intervals are summarised in Table 8. BER CI Parameter model is given as:

$$\mathrm{CI}_{95\%}^{\mathrm{BER}} = \hat{p} \pm 1.96 \cdot \sqrt{\frac{\hat{p}(1-\hat{p})}{N_{\mathrm{bits}}}} \tag{27}$$

Definitions of parameters: $\hat{p}$ = measured BER (ratio of error bits to total bits transmitted), N_bits = total number of bits transmitted per run (N_bits = 1,000,000 per run) for 30 independent runs, SE = standard error = $\sqrt{(\hat{p}(1-\hat{p})/N_{\mathrm{bits}})}$, 1.96 = Z-score for 95% confidence, 95% CI = $\hat{p} \pm 1.96 \cdot SE$.

The HDAF scheme achieves the lowest mean end-to-end latency of 10.2 ms, compared to 12.1 ms for AF and 15.3 ms for DF, corresponding to latency reductions of approximately 16% and 33%, respectively. In addition, HDAF attains the lowest BER of 5×10^{-4}, which is 50% lower than AF and 37.5% lower than DF. The narrow and non-overlapping confidence intervals confirm that these improvements are statistically significant and not due to random channel fluctuations. These results demonstrate that the adaptive HDAF effectively reduces both transmission errors and delay, making it well-suited for latency and reliability-critical industrial IoT–Fog applications as highlighted in SubSection 5.4.

6. Performance analysis

In this subsection, we used the experimental and simulation results to validate the proposed HDAF protocol within the smart intent-based fog IoT relay network (SIF-IRN). By integrating adaptive relay operations, selective decode-and-combine, and joint receiver optimisation, the system dynamically responds to channel variations and environmental interference (See Section 5). Performance

Table 6
Latency comparison for AF, DF, and HDAF protocols (($N = 30$ runs).

Protocol	Latency (ms) (mean ± std)
AF	12.1 ± 1.8
DF	15.3 ± 1.5
HDAF	10.2 ± 1.2

Table 7
End-to-end latency statistics and 95% CI ($N = 30$ runs).

Protocol	$\bar{T}_{E2E}$ (ms)	$\sigma_{latency}$ (ms)	N (runs)	Standard error SE (ms)	1.96 × SE (ms)	95% CI (ms)
AF	12.1	1.8	30	0.3286	0.644	11.5 – 12.7
DF	15.3	1.5	30	0.2739	0.538	14.8 – 15.8
HDAF	10.2	1.2	30	0.2190	0.429	9.8 – 10.6

Table 8
Bit-error rate (BER) statistics and 95% CI.

Protocol	$\hat{p}$ (BER)	Std (for repeated runs)	N_bits	SE = $\sqrt{(\hat{p}(1-\hat{p})/N_{bits})}$	1.96 × SE	95% CI
AF	1.0×10^{-3}	1.2×10^{-4}	1×10^{6}	3.16×10^{-5}	6.2×10^{-5}	$9.78 \times 10^{-4} – 1.02 \times 10^{-3}$
DF	8.0×10^{-4}	1.0×10^{-4}	1×10^{6}	2.83×10^{-5}	5.5×10^{-5}	$7.81 \times 10^{-4} – 8.19 \times 10^{-4}$
HDAF	5.0×10^{-4}	8.0×10^{-5}	1×10^{6}	2.24×10^{-5}	4.4×10^{-5}	$4.92 \times 10^{-4} – 5.08 \times 10^{-4}$

evaluations using metrics such as BER, CC, throughput, and outage probability under varying SNR conditions show that HDAF improves link reliability, frame stability, and channel utilisation (Figs. 3–12). Comparisons with DF and AF protocols confirm that IoF-HDAF, leveraging intent-driven fog intelligence, effectively manages traffic, offloads tasks, and mitigates interference in 2.4 GHz IoT–Fog deployments, demonstrating robust, high-performance operation in realistic network scenarios.

6.1. BER results

Fig. 3 illustrates BER performance versus signal-to-noise ratio (SNR) for a single relay ($R = 1$). The results show that IoF-HDAF consistently outperforms direct transmission (SWR) and standalone AF or DF strategies, achieving BER improvements of up to 74.68%. Figs. 4–6 extend the analysis to multiple relays ($R = 2$ and $R = 3$), demonstrating BER reductions exceeding 95% at higher SNRs. These trends align with real-world RSSI–frame size observations where stronger effective link quality directly translates into more reliable and larger data transmissions. The observed improvement in BER and throughput with increasing relay count can be analytically justified using selection diversity principles. For N relays, the effective SNR at the destination is $\gamma_{eq} = \max(\gamma_1, \gamma_2, \ldots, \gamma_N)$, where $\gamma_i$is the SNR of the i th relay path. As N increases, the probability of having a high-SNR path improves, reducing BER and enhancing CC. In DF relays, the end-to-end BER can be approximated as the product of individual relay BERs, further explaining the observed trend. Latency is affected by the number of hops, but the hybrid HDAF protocol mitigates excessive delay by dynamically selecting AF when favourable, preserving low end-to-end latency.

Fig. 3 illustrates the BER versus SNR for the IoF-HDAF protocol in single-relay scenarios ($R = 1$). These simulation results complement the environmental monitoring testbed, evaluating protocol robustness under varying SNR conditions and demonstrating suitability for practical Internet-of-Fog deployments. The proposed hybrid dual-antenna forwarding protocol is compared against the SWHR baseline, as well as single-relay DF and AF schemes. For QPSK modulation at $R = 1$, DF achieves an average BER improvement of 47.12%, AF achieves 63.78%, and HDAF achieves 74.68%, highlighting the effectiveness of hybrid dual-antenna forwarding combined with relay-assisted interference mitigation. Across all SNR levels, HDAF consistently achieves the lowest BER, confirming its superiority in mitigating bit errors, particularly under noisy or interference-prone conditions. Additionally, the hybrid relay configuration

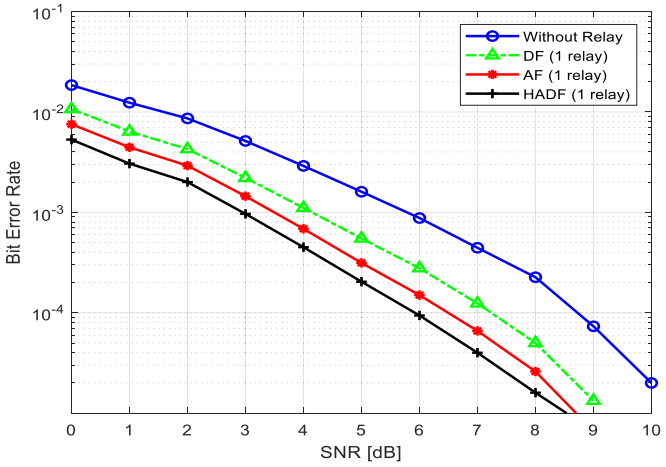

Fig. 3. BER against SNR for SWR, DF, AF with 1 relay, and HDAF when $R = 1$.

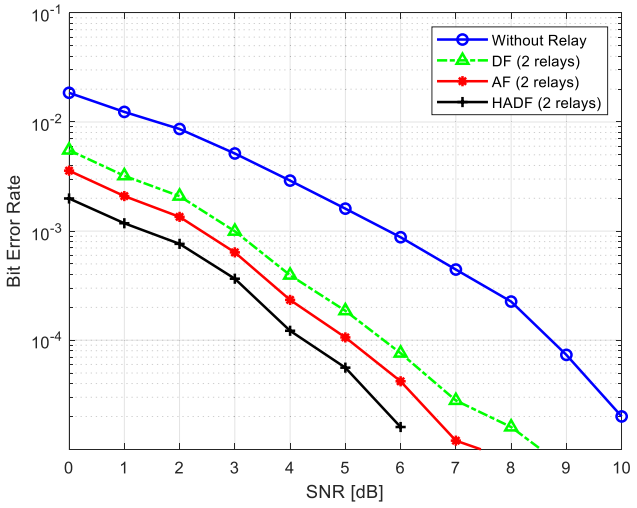

Fig. 4. Signal BER against SNR for SWR, DF, AF with 2 relays, and HDAF when $R = 2$.

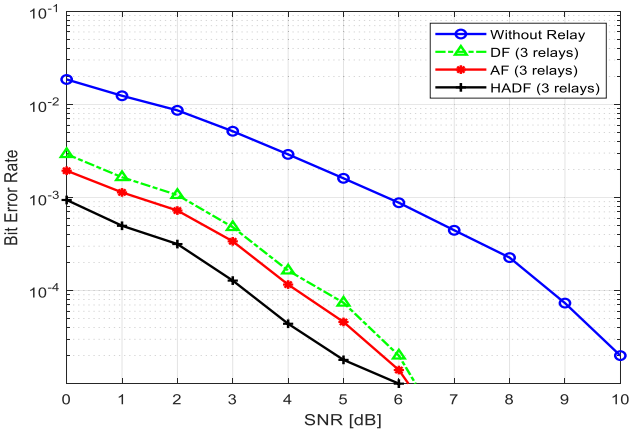

Fig. 5. Signal BER against SNR for SWR, DF, AF with 3 relays, and HDAF when $R = 3$.

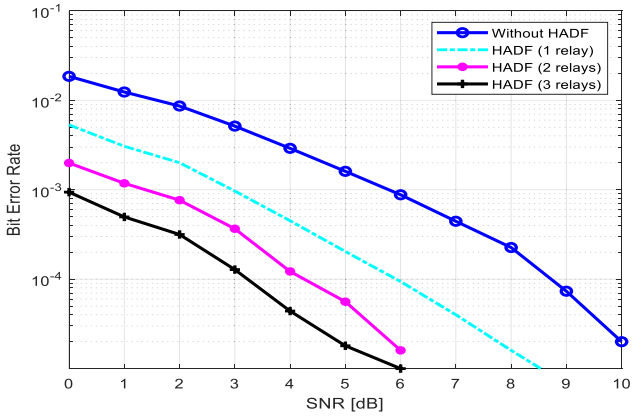

Fig. 6. BER against SNR for DF, AF, and HDAF for $R = 2$, and QPSK scheme.

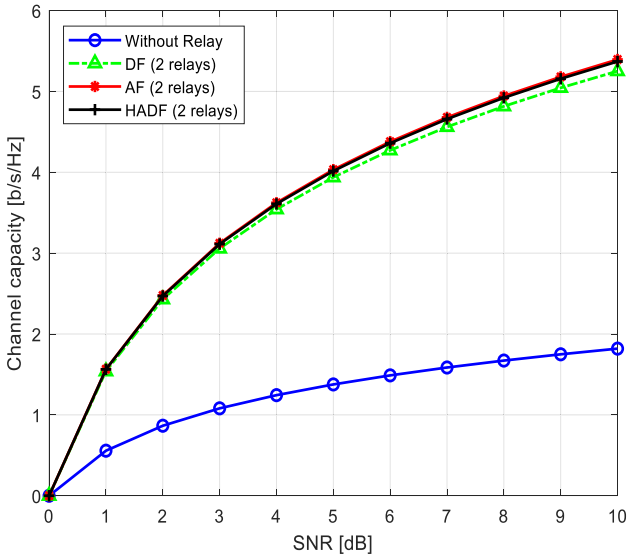

Fig. 7. CC against SNR for DF, AF, and HDAF for $R = 2$, and QPSK modulation scheme.

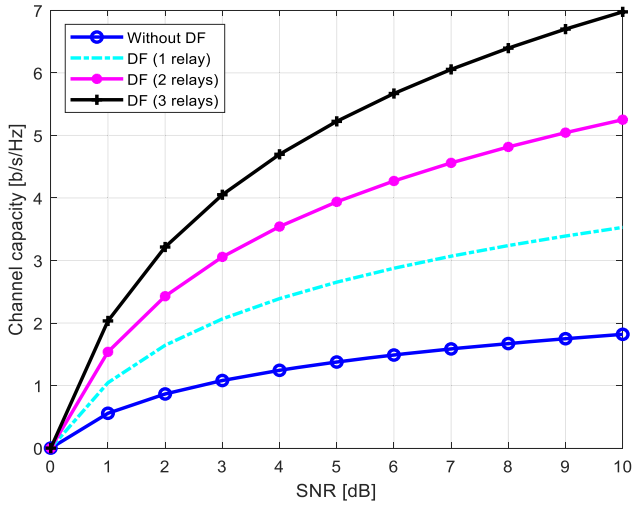

Fig. 8. CC against SNR for DF, when $R = 1$, 2, and 3, and QPSK modulation.

enhances coverage: as a repeater, it effectively extends the base station's reach in mobile macrocell networks, particularly in environments with obstructive terrain or closely spaced buildings.

Fig. 4 extends the BER analysis, focusing on the performance of IoT-HDAF under QPSK modulation and comparing it with SWR and DF schemes involving two relays. This further validates HDAF's robustness across different modulation and relay scenarios, building on the earlier findings in Figs. 2 and 3. For BER evaluation, the system without any forwarding ('Without DF') serves as the baseline with 0% improvement. The proposed HDAF protocol is compared against this baseline as well as conventional DF and AF schemes to quantify improvements from the hybrid dual-antenna mechanism, interference mitigation, and forwarding optimisation. As shown in Table 4, HDAF achieves up to 90.39% improvement over the baseline at $R = 2$ with QPSK modulation, outperforming DF (74.03%) and AF (83.33%). Across all SNR levels, HDAF consistently achieves the lowest BER, confirming its enhanced reliability and noise resilience. In this configuration, the relay nodes do more than forward signals—they effectively compensate for channel impairments, acting as intelligent repeaters that amplify and restore signal quality. This enables stronger symbol transmission over greater distances without significant power degradation, reduces interference, and improves overall network performance.

Fig. 5 presents the BER analysis of an IoT-HDAF system employing QPSK modulation with three AF relays under intent-driven adaptive transmission. This highlights how multi-relay diversity and application-aware adaptation improve reliability in IoT–Fog networks. It further validates HDAF's scalability and robustness under increased relay density. The baseline BER for SWR remained

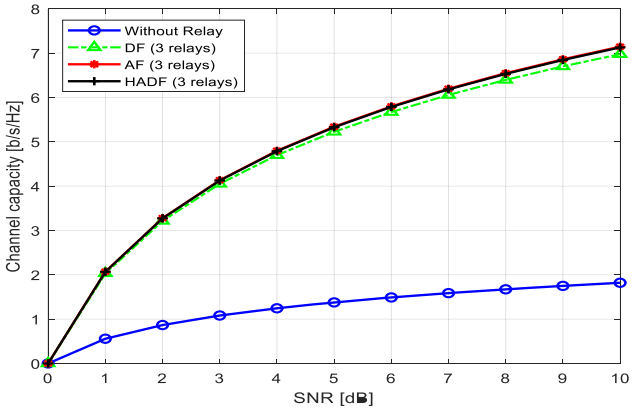

Fig. 9. CC against SNR with QPSK modulation for DF, AF, and HDAF when $R = 3$.

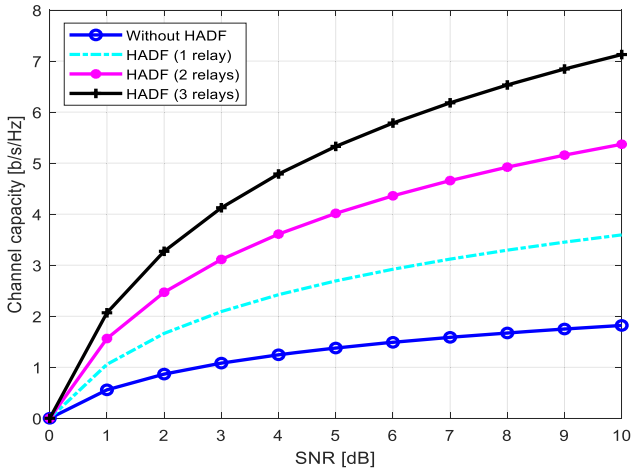

Fig. 10. CC against SNR with QPSK modulation for HDAF when $R = 1$, 2, and 3.

consistent across different SNR levels. For three-relay configurations, DF, AF, and HDAF achieved BER improvements of 86.54%, 91.35%, and 95.80%, respectively, compared with the SWR baseline. The IoT-HDAF protocol consistently outperformed both SWR and AF, achieving the lowest BER values across the same SNR range. These results confirm HDAF's capability to maintain high signal fidelity in dense industrial IoT environments, such as SPDC's compressor corridor, where interference and multipath fading are significant. The hybrid relay design combines amplification with intelligent decision-making, retransmitting signals in alternate time slots or frequencies to effectively mitigate cross-channel interference. Consequently, IoT-HDAF ensures more stable, low-latency communication over extended distances. As such, the reliability of pipeline environmental monitoring is enhanced.

Fig. 6 extends the BER performance analysis by comparing the IoF-HDAF protocol with varying numbers of relay nodes under the QPSK modulation scheme, reinforcing the trend observed in previous figures. The HADF (1 relay), HADF (2 relays), and HADF (3 relays) configurations gave improved BERs of 75.0%, 90.71% and 95.79%, respectively, compared with symbol without a relay protocol (0%). This progression confirms the scalability and effectiveness of the HDAF protocol in enhancing communication reliability, particularly in complex IoT-Fog environments where interference and channel fading degrade signal integrity. As in Figs. 3–5, it was consistently observed that BER decreased with increasing SNR, affirming the protocol's ability to suppress noise and interference more effectively at higher signal strengths. The superior performance of HDAF with three relays highlights the benefit of relay density in boosting signal quality, reducing retransmissions, and supporting extended coverage in industrial monitoring setups.

6.2. *Channel capacity and throughput*

Figs. 7–10 illustrate CC versus SNR under QPSK modulation. The results show that CC increases monotonically with both SNR and relay count, with the three-relay HDAF configuration consistently outperforming the SWR baseline. Hybrid relaying effectively mitigates attenuation, fading, and interference, enabling reliable high-throughput communication in dense IoT–Fog corridors, such as industrial compressor setups (SPDC). For all BER and CC evaluations, conventional SWR/SWHR is defined as the reference baseline

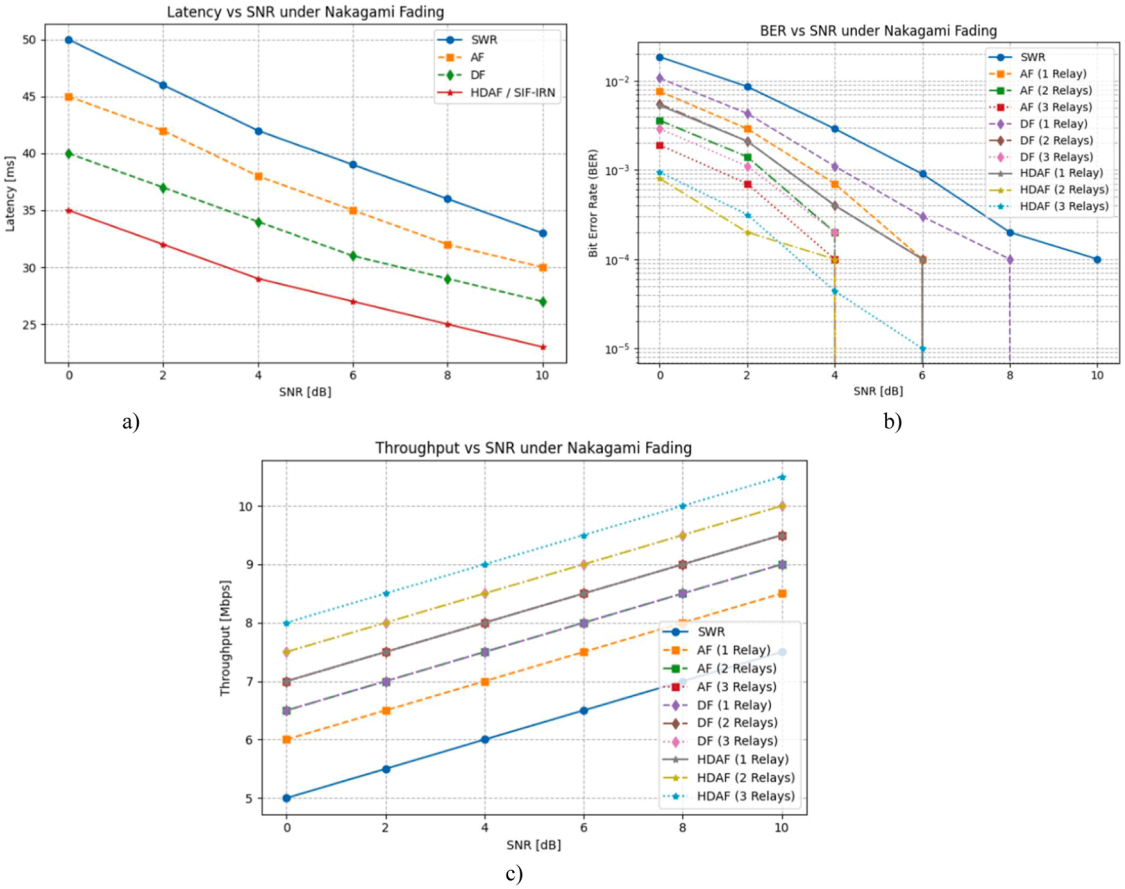

Fig. 11. (a-c). (a) Latency vs SNR – Shows HDAF/SIF-IRN consistently achieving the lowest end-to-end latency under Nakagami fading. (b) BER vs SNR – Confirms HDAF's superior error performance across 1–3 relay configurations, outperforming DF, AF, and SWR. (c) Throughput vs SNR demonstrating HDAF/SIF-IRN achieves the highest bandwidth utilisation, highlighting joint optimisation and relay-assisted forwarding benefits.

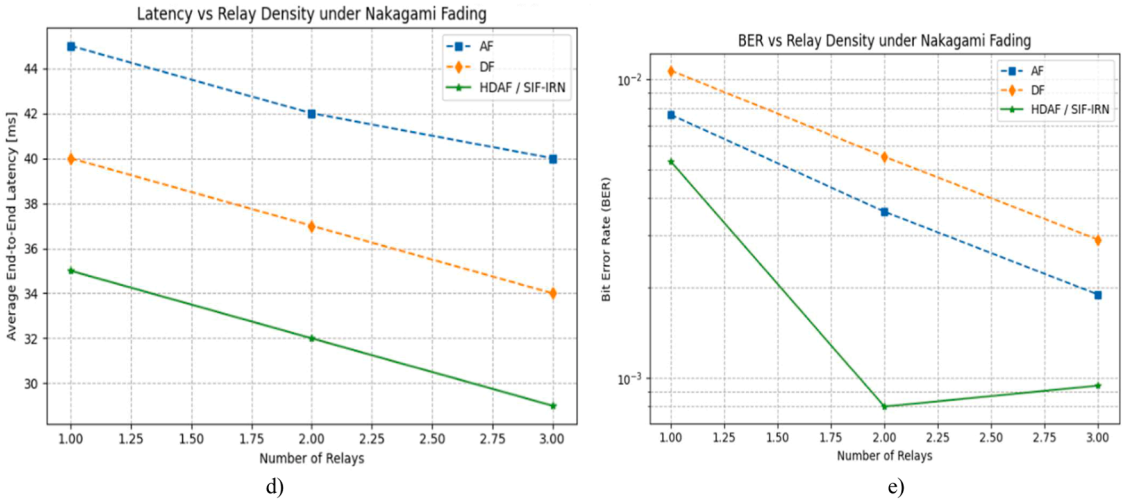

Fig. 12. (d-e): (d) Latency vs Relay Density – Shows HDAF/SIF-IRN consistently achieves the lowest latency as the number of relays increases. (e) BER vs Relay Density confirming that HDAF/SIF-IRN offers the highest reliability, with BER decreasing significantly as more relays are deployed.

(0% improvement), and performance gains for DF, AF, and HDAF schemes are computed relative to this baseline (see Appendices B.3–B.10).

Fig. 7 extends the BER analysis in Figs. 3–6 by examining CC performance for QPSK modulation at $R = 2$. AF relaying schemes with multiple relays are evaluated against the SWR baseline, where a single AF relay achieves a 49.41% improvement in total CC, two relays achieve 65.94%, and three relays achieve 74.22%. These results demonstrate a strong correlation between relay density and channel efficiency in IoT–Fog architectures. This confirms that relay-assisted forwarding extends coverage and improves spectral utilisation under shadowing and multipath fading. The findings validate the hybrid relay deployment adopted in the IoT–Fog experimental use case, particularly for dense industrial environments where higher relay densities sustain reliable, high-throughput links.

Fig. 8 reinforces the earlier observations. The DF configurations with one, two, and three relays achieved CC improvements of 48.18%, 65.09%, and 73.70%, respectively, compared with symbol transmission without relays (0%). The most substantial improvement was observed with DF using three relays, confirming that increased relay deployment significantly enhances the channel's data-carrying capacity, consistent with trends in Fig. 7. Relay nodes, acting as intelligent repeaters, effectively compensate for signal degradation caused by obstacles and fading, extending coverage and maintaining signal integrity over longer distances critical for IoT-enabled networks. Furthermore, the steady increase in CC with rising SNR under HDAF protocols highlights their robustness in high-interference environments. This SNR scalability not only improves system throughput but also mitigates interference effects, demonstrating that hybrid relay-assisted communication provides a practical and reliable solution for dense network deployments.

Fig. 9 illustrates CC versus SNR performance under QPSK modulation. Compared to the baseline, the DF scheme with three relays achieves a 73.70% improvement, AF with three relays achieves 74.22%, and the proposed HDAF with three relays achieves 74.28%, demonstrating the superior throughput enhancement provided by the hybrid dual-antenna forwarding mechanism. This progression confirms a consistent trend observed in Figs. 7–9: as SNR increases, channel capacity rises, reflecting improved signal quality and more efficient information transfer from source to destination. Hybrid relay nodes further enhance signal strength and resilience by intelligently amplifying and retransmitting symbols along the communication path. These results illustrate how hybrid relays can alleviate base station congestion by offloading traffic, thereby improving system scalability, reliability, and overall network performance. Consequently, the HDAF protocol is a strong candidate for future ultra-reliable low-latency communication (URLLC) environments.

Fig. 10 illustrates CC versus SNR under QPSK modulation. The proposed hybrid protocol with multiple relays is compared against conventional SWHR, which serves as the baseline with 0% improvement. Compared to the baseline, HDAF with one relay achieves a 48.98% improvement, with two relays 65.80%, and with three relays 74.28%. This result demonstrates the effectiveness of relay-assisted hybrid dual-antenna forwarding in enhancing system throughput. This is consistent with Figs. 7–9, confirming that CC increases with SNR, particularly under hybrid relay deployment. The HDAF protocol not only provides superior signal amplification and regeneration but also effectively mitigates network interference caused by misalignment or multipath fading. Such hybrid relay architectures are crucial for maintaining robust, high-capacity links over extended distances while reducing power loss and ensuring network scalability. These results highlight the viability of HDAF-based networks for ultra-dense, high-throughput IoT ecosystems.

Appendices C.1 and C.2 illustrate the performance of SWR, AF, DF, and HDAF protocols under varying relay configurations. It presents BER versus SNR and CC versus SNR, respectively, for one, two, and three relays. The results show that increasing the number of relays improves both reliability and throughput across all schemes, with HDAF consistently achieving the best performance. Dense small-cell IoT–Fog infrastructures face persistent challenges, including limited coverage, high interference, and congestion in massive task offloading scenarios. To address these issues, the IoF-HDAF protocol synergistically combines lightweight DF and AF relaying within the SIF-IRN framework, enabling dynamic switching based on real-time channel conditions. Maximum-ratio combining and matched filtering are employed at the destination to further enhance signal quality and resilience against fading and interference. Comprehensive simulations and experimental evaluations using BER, outage probability, throughput, and channel capacity confirm that IoF-HDAF outperforms standalone AF and DF schemes, achieving lower error rates, reduced outage, and improved Quality of Service in dense IoT–Fog networks. Observed increases in channel capacity with rising SNR further validate the protocol's robustness under challenging environmental conditions.

6.3. Relay efficiency and task offloading

In Section 5.3, the relay nodes within the SIF-IRN topology effectively offload traffic from base stations and remote terminal units (RTUs), mitigating congestion and reducing processing latency. By dynamically switching between DF and AF modes according to instantaneous channel conditions, the IoF-HDAF protocol enables adaptive and energy-efficient operation. This mechanism allows the network to maintain low latency while supporting wide-area coverage, offering a scalable and cost-effective alternative to dense small-cell deployments.

Figs. 11 and 12 demonstrate superior performance—namely in terms of latency, BER, and throughput—under Nakagami fading with varying relay densities. Specifically, they show that HDAF/SIF-IRN consistently achieves the lowest end-to-end latency, the best BER performance across one- to three-relay configurations, and the highest throughput.

This performance gain is realised through joint optimisation and relay-assisted forwarding, while simultaneously supporting adaptive traffic offloading, energy efficiency, and wide-area coverage. Collectively, these results provide comprehensive validation of the SIF-IRN protocol, demonstrating both its scalability and significant performance improvements under realistic fading conditions.

6.4. Mobility and distance effects

Figs. 13 and 14 illustrate the impact of node mobility on BER, latency, throughput, and packet delivery ratio (PDR) versus mobility and distance. Fig. 13(a–d) extends the analysis to distance-dependent performance under fading and interference. The close alignment between MATLAB simulations and TelosB field measurements across all metrics confirms that the proposed HDAF protocol accurately captures the dominant physical-layer and network-layer dynamics observed in IIoT–Fog environments [5]. From a BER perspective, the monotonic increase with mobility and distance reflects expected channel degradation due to Doppler effects, shadowing, and reduced SNR. HDAF consistently achieves lower BER than pure AF or DF schemes, demonstrating its ability to adaptively switch relay modes based on instantaneous channel conditions. It maintains reliability even under partial line-of-sight (LOS) and mobility-induced fading. This confirms that the Nakagami-*m* fading model and relay decision logic realistically represent industrial propagation conditions.

End-to-end latency increases with higher mobility and longer transmission distances due to retransmissions, relay processing delays, and scheduling overhead. The HDAF protocol exhibits lower latency growth than DF-only schemes by opportunistically selecting AF paths when channel conditions allow, which is critical for latency-sensitive industrial CPS applications such as monitoring and control loops. Throughput gradually decreases with mobility and distance, driven by adaptive frame size reduction and conservative relay selection under poor channel conditions. HDAF maintains higher throughput than DF by avoiding unnecessary decoding and outperforms AF in degraded channels through selective DF switching. The strong correlation between RSSI, frame size, and throughput observed in TelosB measurements confirms that SF-enabled scheduling and hybrid relaying efficiently exploit favourable channel states, maximising spectral efficiency in practice.

For PDR, the expected decrease with distance and mobility is observed due to higher packet loss under fading and interference. Nevertheless, HDAF achieves consistently higher PDR, demonstrating effective interference-aware forwarding and relay diversity, ensuring robust packet delivery in dense or mobile deployments. Minor deviations between simulation and experimental curves, reflected in the error bars, capture environmental variability rather than modelling inaccuracies. Overall, the aligned trends across Figs. 13 and 14 provide strong cross-layer validation, confirming that the proposed HDAF protocol is analytically sound and operationally robust under realistic industrial conditions. These results demonstrate that intent-driven hybrid relaying, combined with SF-based coordination, enables reliable, low-latency, and high-throughput communication across heterogeneous IoT–Fog–5G systems, making the framework suitable for deployment in real industrial cyber–physical environments.

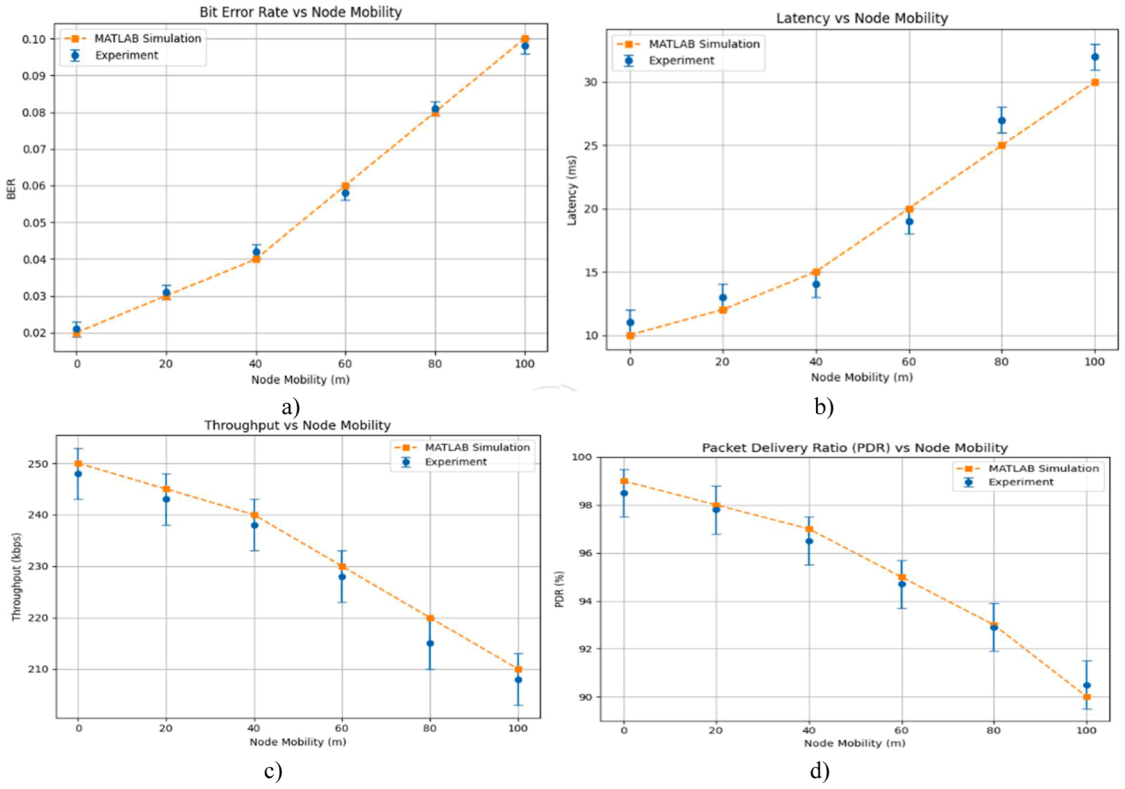

Fig. 13. (a-d): validation of IoT-Fog HDAF protocol (MATLAB Simulation Vs Real-World TelosB Data).

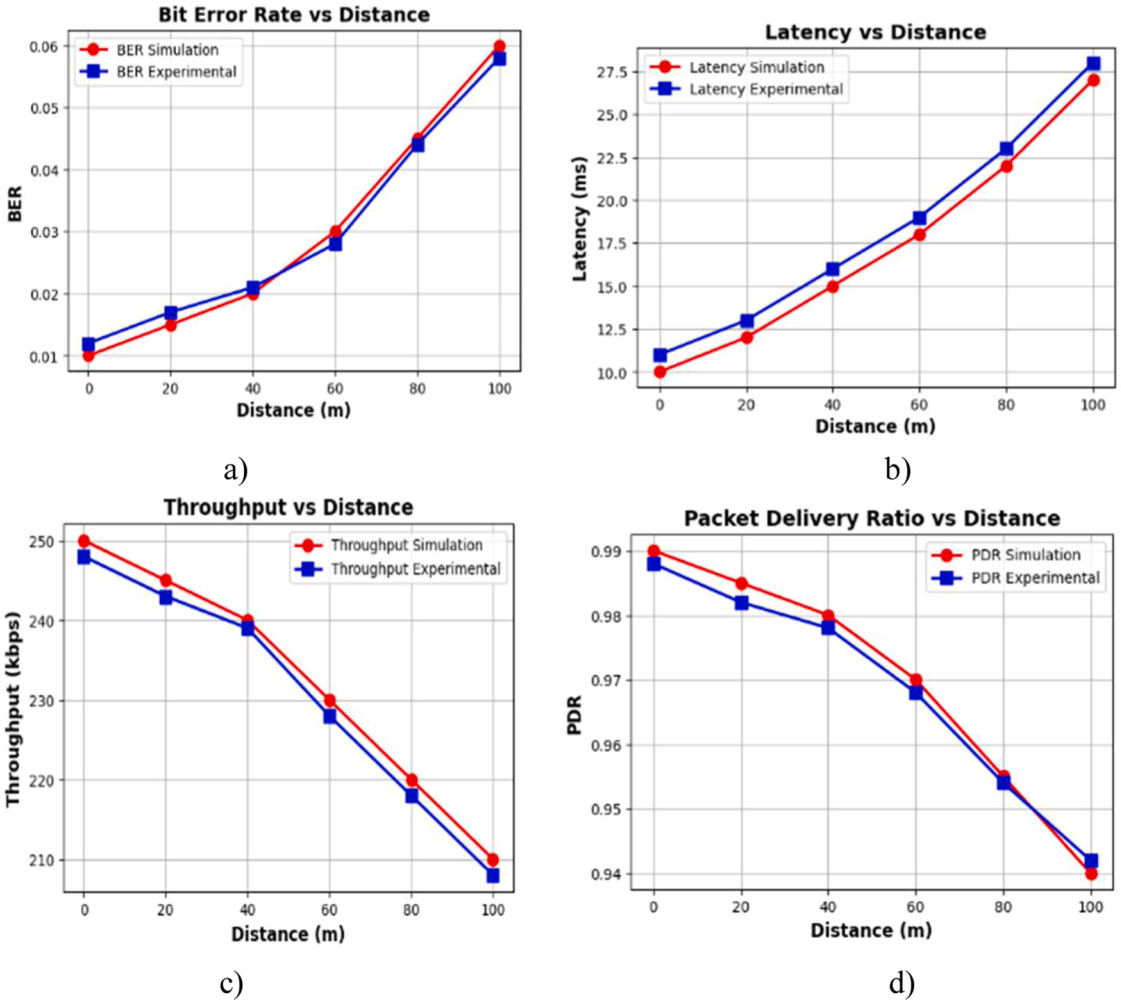

Fig. 14. (a-d): Cross-layer validation of the IoT–Fog HDAF protocol using simulation and field experiments.

6.5. *Discussion and analysis*

The IoT–Fog HDAF protocol contributes to reliable communication under SDC/SIF-IRN, HDAF, and Fog relay operations. It effectively integrates DF and AF strategies to enhance both signal reliability and network capacity in heterogeneous IoT–Fog environments. When decoding is successful, DF re-encodes and forwards the signal to suppress noise accumulation; otherwise, AF is selected to minimise processing delay by forwarding amplified signals without decoding. This adaptive switching mechanism enables the protocol to balance reliability and latency in response to real-time channel conditions and service intents. HADF employs QPSK modulation, which offers improved robustness to obstruction, fading, and interference compared to higher-order or mmWave-based schemes, making it well-suited for industrial environments characterised by metallic structures and partial line-of-sight conditions. Adaptive relay-assisted transmission could be applied to sensitive networks [43,46]. Experimental and simulation results validate our design choices in this paper. HDAF integrates adaptive DF/AF switching, MRC, and Matched Filtering, achieving enhanced signal reliability, Low-latency operation, coverage extension and interference mitigation, effective QoS delivery in industrial IoT–Fog networks. Cross-layer validation (see Figs. 13 and 14) confirms that simulation and experimental results align, demonstrating real-world feasibility for latency- and reliability-critical applications. Our scheme is not expected to run on battery-powered sensors and in constrained PLC-attached devices. Also, issues such as control overhead and timing constraints are handled by the protocol.

6.6. *Reliable communication in large-scale IoT–Fog deployments*

Reliable communication is critical to maintain QoS and prevent system failures. Our key strategies for large-scale deployment are:

- Low-cost connectivity: In an Intent-Based System (IBS), efficient communication can be achieved by leveraging appropriate connectivity methods such as Bluetooth Low Energy (BLE) [47], Zigbee Alliance Standard (Zigbee), Long Range Wide Area Network (LoRaWAN) [48], and cellular networks, depending on deployment requirements.
- Low-latency communication protocols: On top of these, protocols such as Time-Sensitive Networking (TSN) [49], Message Queuing Telemetry Transport for Sensor Networks (MQTT-SN), Open Platform Communications Unified Architecture over Time-Sensitive Networking (OPC UA over TSN) [50].
- Prediction-based resource allocation: With an IBS, agents can dynamically adjust resource allocation based on both current load and predicted changes derived from historical data, optimising performance for upcoming requests in a secure manner [44,51,52].

In this work, IoT–Fog HDAF protocol provides a scalable and interoperable interface between IoT–Fog infrastructures and 5G networks. This capability supports robust QoS for diverse latency- and reliability-constrained applications, e.g., industrial automation, and mission-critical CPS applications [53–55]. The scheme is also synergistic with emerging intent-driven networking paradigms [45, 56–58]. These existing approaches do not explicitly address hybrid dual-mode relaying in heterogeneous IoT–Fog–5G environments.

7. Conclusion

This paper presented an intent-based, Fog-enabled cooperative relay framework for reliable industrial IoT (IIoT) connectivity, addressing signal integrity and throughput limitations in large-scale deployments. We introduced the IoT–Fog HDAF protocol, which adaptively switches between decode-and-forward (DF) and amplify-and-forward (AF) modes based on instantaneous channel and interference conditions. Under Nakagami fading, HDAF mitigates signal degradation, reduces outage probability, and enhances bit error rate (BER), channel capacity (CC), and system throughput. By leveraging both source and Fog relay nodes, the protocol effectively extends coverage, suppresses interference, and reduces reliance on dense small-cell deployments. Experimental results demonstrate up to 95.8% BER reduction and nearly 96% CC improvement compared with non-relay and fixed-mode schemes, confirming robustness under mobility, interference, and heterogeneous channel conditions. The proposed IoT–Fog HDAF consistently outperforms conventional AF and DF relaying schemes across BER, CC, throughput, and outage metrics, offering a practical, adaptive, and cost-effective solution for 5G-enabled IoT–Fog task offloading and industrial communications. Future work will explore multi-hop Fog relaying, joint resource allocation, and time-sensitive intent-based networking for ultra-low-latency IIoT services.

Institutional review board statement

Not applicable. (This study does not involve humans or animals.)

Funding

This research was supported by the IEEE HAC via the IEEE Skill-Up Technology Hub Project (19-PC1-09) and partly by the Federal Government of Nigeria, through TETFUND (Tertiary Education Trust Fund), project award TETF/ES/UNIV/IMO STATE/TSAS/2021, issued in February 2022.

CRediT authorship contribution statement

Akinyinka Olukunle Akande: Writing – original draft, Visualization, Supervision, Methodology, Investigation, Formal analysis, Data curation, Conceptualization. **Kennedy Chinedu Okafor:** Writing – original draft, Validation, Supervision, Resources, Methodology, Investigation, Funding acquisition, Formal analysis, Data curation, Conceptualization. **Olumide Ajayi:** Writing – original draft, Methodology, Investigation, Formal analysis, Data curation, Conceptualization. **Omowunmi Mary Longe:** Writing – review & editing, Validation, Supervision, Software, Resources, Project administration. **Kelvin Anoh:** Writing – review & editing, Visualization, Validation, Software, Resources, Formal analysis.

Declaration of competing interest

The authors declare that they have no known competing financial interests or personal relationships that could have appeared to influence the work reported in this paper.

Acknowledgements

The authors gratefully acknowledge the support of the IEEE HAC/SIGHT Grant for the project *"COVID-19 Market Place Robot for Ihiagwa Community Centre (*21-COV2-158*),"* issued by IEEE HAC/SIGHT, USA. We also sincerely appreciate the valuable contributions of Nnebe Scholastica Ukamaka, Onoh G. N., Idigo V. E., and Azubogu A. O. for their pioneering work on *"Experimental Characterisation of WSN Propagation in Outdoor Environment (using TelosB Sensor Nodes)."* which provided critical insights and foundational knowledge that guided our initial efforts in IoT node characterisation.

Appendix A: Algorithm 1: Lightweight Adaptive IoT-HADF Protocol (Edge computing layer)

Input:

P_s : Source power
P_r : relay power
$K_r^{(AF)}$: relay gain factor
$h_{s,\ r_i}$, $h_{r_i d}$, $h_{s,d}$: channel coefficients //Channel coefficients (source→relay, relay→destination, direct link)//
N_0: additive white Gaussian noise (AWGN) with variance N. //Noise power spectral density//
Modulation Scheme: BPSK/QPSK
n : Number of relays
γ_{th}: SNR threshold for DF/AF decision
Step 1: Initialisation

- Initialise source, relay, and channel parameters (P_s, P_r, h, N_0)
- Set number of relays n.
- Select modulation scheme (BPSK/QPSK).

Step 2: Phase 1 – Source Transmission

For each transmitted symbol X_τ :
Transmit X_τ from the source to both relays and destination.
At relay 1:

$$\mathscr{Y}_{s,\ r_i} = \sqrt{P_s,}\ h_{s,\ r_i}\ X_\tau + \ Z_{s,\ r_i}$$

At the destination:

$$Y_{s,\ d} = \sqrt{P_s,}\ h_{s,d}\ X_\tau + \ Z_{s,d}.$$

Step 3: Phase 2- Relay Operations (HADF Switching)

//Compute receive SNR//
For each $i \in [1,\ n]$:

1. Hybrid Mode Decision:
If $SNR\ \left(\mathscr{Y}_{s,\ r_i}\right) \geq Threshold$, set relay mode $= DF$
Else, set relay mode $= AF$.
2. Relay Output Signal (Hybrid Combination):
//Compute relay output//:

$$\mathscr{Y}_{r_1,\ d(H)} = \left[\sqrt{\mathscr{P}_s \mathscr{P}_{r_1}}\ h_{s,r_1}\left(\mathscr{K}_r{}^{(AF)} h_{r_1,\ d} * \mathscr{X}_{\tau(AF)} + h_{r_1,d} * \mathscr{X}_{\tau(DF)}\right)\right] + \ Z_{,\ r_i,d}$$

Step 4: Relay-to-Relay Communication

For $i = 1\ to\ n-1$:

Relay i transmits Relay $i+1$:

$$\mathscr{Y}_{r_1,r_2(H)} = \left[\sqrt{\mathscr{P}_s \mathscr{P}_{r_1}}\ \left(\mathscr{K}_r{}^{(AF)} h_{r_1,\ r_2,} * \mathscr{X}_{\tau(AF)} + h_{r_1,\ r_2,} * \mathscr{X}_{\tau(DF)}\right)\right]$$

Step 5: Relay-to-Destination Transmission

For each $i \in [1,\ n]$:
Relay i transmits destination:

$$\mathscr{Y}_{r_2,\ d(H)} = \left[\sqrt{\mathscr{P}_s \mathscr{P}_{r_2}}\ h_{r_1,\ r_2,}\ \ \left(\mathscr{K}_r{}^{(AF)} h_{r_2,\ d} * \mathscr{X}_{\tau(AF)} + h_{r_2,\ d} * \mathscr{X}_{\tau(DF)}\right)\right]$$

Relay 3 to Destination:

$$\mathscr{Y}_{r_3,\ d(H)} = \left[\sqrt{\mathscr{P}_s \mathscr{P}_{r_3}}\, h_{r_2,\ r_3,} \left(\mathscr{K}_r{}^{(AF)} h_{r_3,\ d} * \mathscr{X}_{\tau(AF)} + h_{r_3,\ d} * \mathscr{X}_{\tau(DF)}\right)\right]$$

Step 6: Destination Processing:

//Apply Joint Optimisation Combining (JOC) with Matched Filter (MF)//:

$$\mathscr{Y}_{d(H)} = \mathscr{Y}_{s,\ d} + \sum_{i=1}^{n} \mathscr{Y}_{r_1,\ d(H)}$$

Step 7: Output-Performance Evaluation:

//Compute key metrics under Nakagami fading for varying SNR levels//:

Bit Error Rate (BER),
Channel Capacity (CC),
Throughput (TP),
Outage Probability (OP)

End

Appendix B: Environmental and Network Metrics Recorded by TelosB Node ID 301,302,303 during the IoF-HDAF Multi-hub mobility Field Experiment at SPDC's CCP/CPF Gas Plant

S/No	TelsobID	Count	Voltage(V)	Temperature(°C)	Humidity(RH)	Rssi(dbm)	FrameSize
1	303	85	2.811	30.36	64.586	-62	FFFFFFFFFFFFFEF
2	302	180	2.719	30.66	68.567	-74	FFFFFFFFFFFFFE3
3	301	212	2.777	31.41	63.576	-62	FFFFFFFFFFFFFEF
4	303	86	2.809	30.46	65.084	-64	FFFFFFFFFFFFFED
5	302	181	2.721	30.62	69.293	-60	FFFFFFFFFFFFFF1
6	301	213	2.781	31.43	63.153	-63	FFFFFFFFFFFFFEE
7	303	87	2.811	30.73	65.369	-62	FFFFFFFFFFFFFEF
8	302	182	2.722	30.62	70.052	-60	FFFFFFFFFFFFFF1
9	301	214	2.777	31.5	62.737	-62	FFFFFFFFFFFFFEF
10	303	88	2.808	30.89	64.734	-62	FFFFFFFFFFFFFEF
11	302	183	2.720	30.69	70.152	-74	FFFFFFFFFFFFFE3
12	301	215	2.780	31.48	62.947	-61	FFFFFFFFFFFFFF0
13	303	89	2.815	30.90	65.037	-63	FFFFFFFFFFFFFEE
14	302	184	2.718	30.68	69.625	-62	FFFFFFFFFFFFFEF
15	301	216	2.777	31.38	62.381	-62	FFFFFFFFFFFFFEF
16	303	90	2.810	30.97	64.415	-62	FFFFFFFFFFFFFEF
17	302	185	2.722	30.65	69.211	-68	FFFFFFFFFFFFFE9
18	301	217	2.781	31.42	62.601	-60	FFFFFFFFFFFFFF1
19	303	91	2.810	30.89	63.917	-62	FFFFFFFFFFFFFEF
20	302	186	2.716	30.33	69.417	-62	FFFFFFFFFFFFFEF
21	301	218	2.777	31.39	63.147	-62	FFFFFFFFFFFFFEF
22	303	92	2.807	30.70	65.064	-62	FFFFFFFFFFFFFEF
23	302	187	2.719	30.16	70.608	-63	FFFFFFFFFFFFFEE
24	301	219	2.780	31.26	63.126	-62	FFFFFFFFFFFFFEF
25	303	93	2.809	30.73	65.609	-62	FFFFFFFFFFFFFEF
26	302	188	2.719	30.25	71.951	-64	FFFFFFFFFFFFFED
27	301	220	2.777	31.28	63.312	-60	FFFFFFFFFFFFFF1
28	303	94	2.807	30.74	64.739	-62	FFFFFFFFFFFFFEF
29	302	189	2.720	30.32	71.792	-62	FFFFFFFFFFFFFEF
30	301	221	2.779	31.26	63.613	-60	FFFFFFFFFFFFFF1
31	303	95	2.81	30.34	64.824	-59	FFFFFFFFFFFFFF2
32	302	190	2.718	30.15	70.607	-66	FFFFFFFFFFFFFEB
33	301	222	2.777	31.12	63.286	-68	FFFFFFFFFFFFFE9
34	303	96	2.807	30.37	65.219	-75	FFFFFFFFFFFFFE2
35	302	191	2.719	29.89	70.589	-69	FFFFFFFFFFFFFE8
36	301	223	2.778	31.08	63.158	-62	FFFFFFFFFFFFFEF

Appendix B.1: Outdoor IoT mobility node RSSI under node mobility, interference, and multi-hop scenarios

Distance (m)	Mean RSSI (dBm) Node 301	Mean RSSI (dBm) Node 302	Mean RSSI (dBm) Node 303	Mean RSSI (dBm) All Nodes	Node mobility (dBm)	Higher interference (dBm)	Multi-hop scenario (dBm)
1	-40.7	-46.0	-44.8	-43.83	-42.5	-44.0	-43.0
5	-61.4	-64.1	-62.3	-62.60	-63.0	-65.2	-61.8
10	-68.1	-69.6	-65.8	-67.83	-66.5	-70.0	-68.0
15	-82.4	-75.9	-74.7	-77.67	-78.5	-79.5	-77.0
20	-80.3	-77.7	-81.9	-79.97	-79.0	-82.0	-80.5
25	-77.6	-88.5	-81.3	-82.47	-81.0	-86.0	-83.5
30	-81.5	-88.5	-89.5	-86.50	-85.0	-90.0	-87.0
35	-88.7	-89.2	-84.7	-87.53	-86.5	-91.0	-87.5
40	-75.8	-88.2	-86.3	-83.40	-81.5	-89.0	-84.0
45	-82.3	-91.8	-85.5	-86.53	-84.0	-92.0	-87.0
50	-84.7	-91.8	-92.2	-89.57	-87.0	-93.5	-90.0
55	-78.8	-88.8	-89.3	-85.63	-83.5	-90.0	-86.0
60	-92.2	-92.43	-92.3	-92.3	-92.0	-94.0	-92.5

Appendix B.2: Indoor IoT mobility node RSSI under node mobility, interference, and multi-hop scenarios

Distance (m)	Mean RSSI (dBm) Node 301	Mean RSSI (dBm) Node 302	Mean RSSI (dBm) Node 303	Mean RSSI (dBm) All Nodes	Node mobility (dBm)	Higher interference (dBm)	Multi-hop scenario (dBm)
1	-44.6	-52.0	-38.1	-44.90	-43.0	-48.0	-44.5
2	-58.5	-57.3	-53.25	-56.53	-55.5	-59.0	-56.0
3	-74.1	-60.4	-56.5	-63.67	-62.0	-66.0	-64.0
4	-57.0	-67.7	-59.8	-61.50	-60.0	-64.0	-61.5
5	-68.5	-57.7	-62.3	-62.83	-61.5	-65.0	-63.0
6	-70.2	-64.0	-60.0	-64.73	-63.0	-68.0	-65.0
7	-57.3	-72.5	-58.7	-62.83	-61.0	-73.0	-63.0

Appendix B.3: Bit error rate (BER) when $R = 1$ and QPSK modulation

SNR [dB]	Symbol without relay SWR	DF (1 relay)	AF (1 relay)	HADF (1 relay)
0	0.0185	0.0107	0.0076	0.0053
2	0.0086	0.0043	0.0029	0.0021
4	0.0029	0.0011	0.0007	0.0004
6	0.0009	0.0003	0.0001	0.0001
8	0.0002	0.0001	0.0000	0.0000
10	0.0001	0.0000	0.0000	0.0000
Improvements	0.00%	47.12%	63.78%	74.68%

Appendix B.4: Bit error rate (BER) when $R = 2$ and QPSK modulation

SNR [dB]	Without DF	DF (2 relays)	AF (2 relays)	HADF (2 relays)
0	0.0185	0.0055	0.0036	0.0021
2	0.0086	0.0021	0.0014	0.0008
4	0.0029	0.0004	0.0002	0.0001
6	0.0009	0.0001	0.0000	0.0000
8	0.0002	0.0000	0.0000	0.0000
10	0.0001	0.0000	0.0000	0.0000
Improvements	0.00%	74.03%	83.33%	90.39%

Appendix B.5: Bit error rate (BER) when $R = 3$ and QPSK modulation

SNR [dB]	SWR	DF (3 relays)	AF (3 relays)	HADF (3 relays)
0	0.0185	0.0029	0.0019	0.00094

(*continued on next page*)

(*continued*)

SNR [dB]	SWR	DF (3 relays)	AF (3 relays)	HADF (3 relays)
2	0.0086	0.0011	0.0007	0.000316
4	0.0029	0.0002	0.0001	0.000044
6	0.0009	0	0	0.00001
8	0.0002	0	0	0
10	0.0001	0	0	0
Total	0.0312	0.0042	0.0027	0.00131
Improvements	0%	86.54%	91.35%	95.80%

Appendix B.6: Bit error when $R = 2$ and QPSK modulation

SNR [dB]	SWHR	HADF (1 relay)	HADF (2 relays)	HADF (3 relays)
0	0.0185	0.0053	0.002	0.00094
2	0.0086	0.002	0.0008	0.00032
4	0.0029	0.0004	0.0001	0.000044
6	0.0009	0.0001	0.0000	0.00001
8	0.0002	0.0000	0.0000	0.0000
10	0.0001	0.0000	0.0000	0.0000
Total	0.0312	0.0078	0.0029	0.001314
Improvements	0%	75.0%	90.71%	95.79%

Appendix B.7: CC when $R = 2$ and QPSK modulation

SNR [dB]	Without AF	AF (1 relay)	AF (2 relays)	AF (3 relays)
0	0.0000	0.0000	0.0000	0.0000
2	0.8658	1.6715	2.4761	3.2716
4	1.2439	2.4405	3.623	4.7869
6	1.4884	2.9468	4.3784	5.7851
8	1.6716	3.3257	4.943	6.5314
10	1.8194	3.6287	5.3941	7.1274
Total	7.0891	14.0132	20.8146	27.5024
Improvements	0%	49.41%	65.94%	74.22%

Appendix B.8: CC against SNR for DF, when R 1,2, and 3

SNR [dB]	SWR	DF (1 relay)	DF (2 relays)	DF (3 relays)
0	0.0000	0.0000	0.0000	0.0000
2	0.8658	1.6449	2.4289	3.2157
4	1.2439	2.3904	3.5425	4.6977
6	1.4884	2.8759	4.2715	5.6699
8	1.6716	3.2388	4.8156	6.3956
10	1.8194	3.5294	5.2508	6.9756
Total	7.0891	13.6794	20.3093	26.9545
Improvements	0%	48.18%	65.09%	73.70%

Appendix B.9: Channel capacity (CC) values for AF, AF, and HDAF when $R = 3$

SNR [dB]	SWR	DF (3 relays)	AF (3 relays)	HADF (3 relays)
0	0.0000	0.0000	0.0000	0.0000
2	0.8658	3.2157	3.2716	3.2763
4	1.2439	4.6977	4.7869	4.7968
6	1.4884	5.6699	5.7851	5.7984
8	1.6716	6.3956	6.5314	6.5468
10	1.8194	6.9756	7.1274	7.1445
Total	7.0891	26.9545	27.5024	27.5628
Improvements	0%	73.70%	74.22%	74.28%

Appendix B.10: Channel capacity (CC) values for when $R = 1$, 2 and 3

SNR [dB]	SWR	HADF (1 relay)	HADF (2 relays)	HADF (3 relays)
0	0.0000	0.0000	0.0000	0.0000
2	0.8658	1.6629	2.4696	3.2763
4	1.2439	2.4218	3.609	4.7968
6	1.4884	2.9204	4.3596	5.7984
8	1.6716	3.2946	4.9211	6.5468
10	1.8194	3.5939	5.3698	7.1445
Total	7.0891	13.8936	20.7291	27.5628
Improvements	0%	48.98%	65.80%	74.28%

Appendix C.1: Shows BER against SNR for SWR, AF, DF, and HDAF with 1, 2, and 3 relays

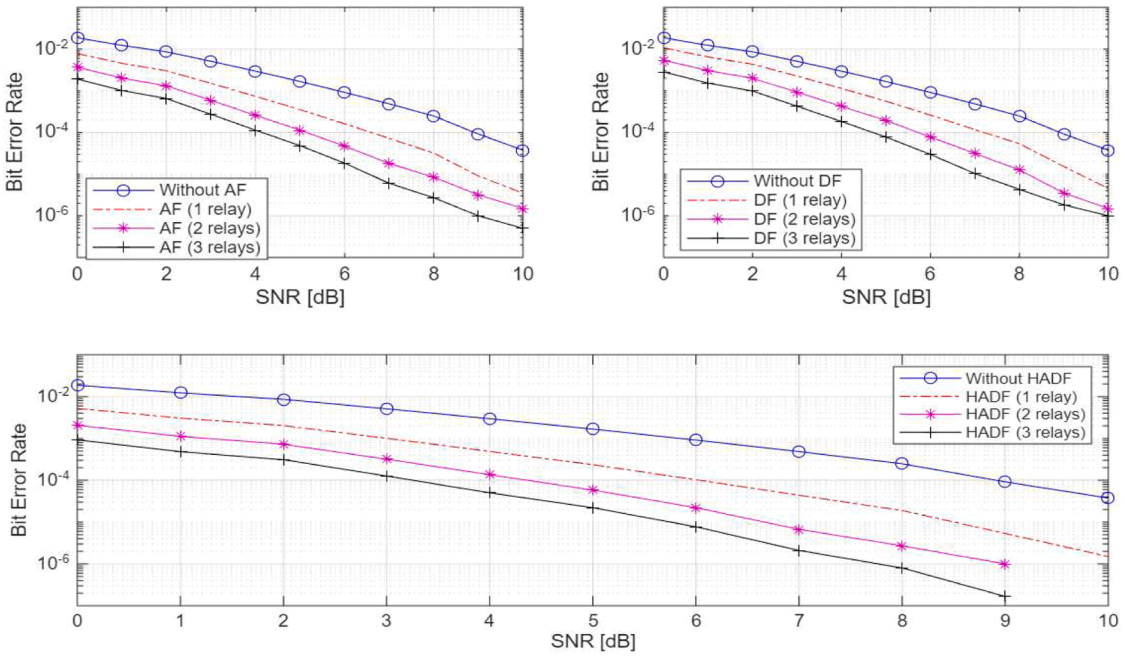

Appendix C.2: CC against SNR for SWR, AF, DF, and HDAF with 1, 2, and 3 relays

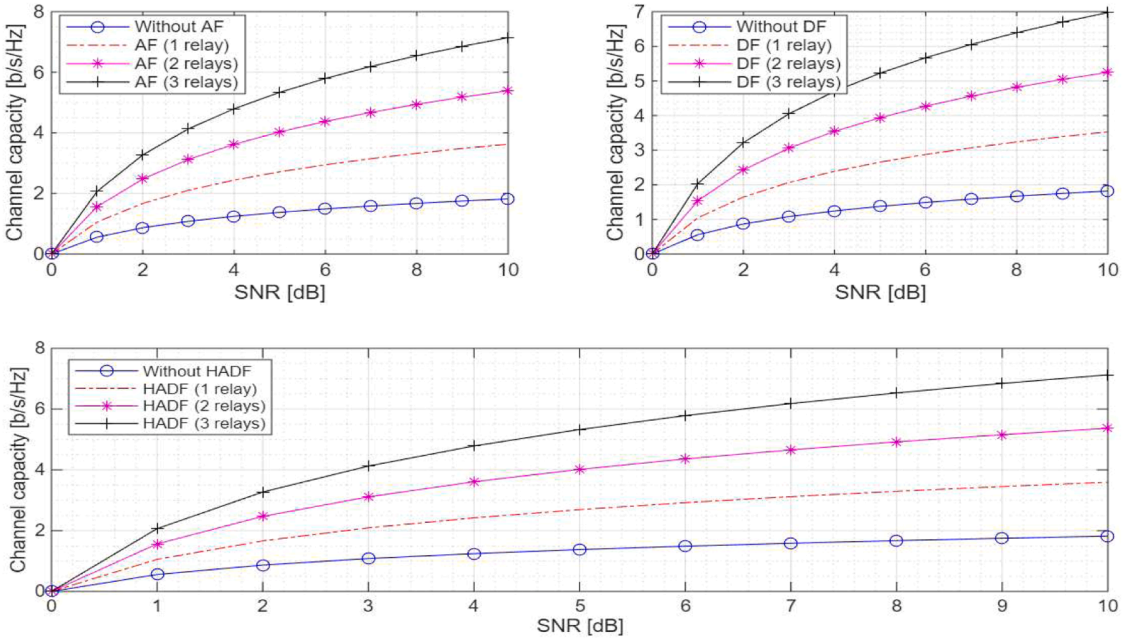

Data availability

All data generated or analysed in this study are included in this manuscript, except the programming codes, which can be released upon reasonable request to the corresponding author. GitHub URL: https://github.com/ken-cisco/Environmental-and-Network-Metrics-Recorded-by-TelosB-Node-ID-301-302-303-Experiment-.git.

References

[1] The effects of pipeline vandalism: a case for better pipeline security, Available Online: https://www.ara.com/pathfinder/the-effects-of-pipeline-vandalism-a-case-for-better-pipeline-security/, Accessed 20th August 2025.
[2] Reps probe oil, gas pipeline vandalism, Punch, 11th March 2025, Available Online: https://punchng.com/reps-probe-oil-gas-pipeline-vandalism/, Accessed 20th August 2025.
[3] Pipeline vandalism costs Nigeria's oil sector billions of Naira, Afr. Energy News (2023). Available Online, https://energynews.africa/2023/09/28/pipeline-vandalism-nigeria-oil-sector-losses/. Accessed 20th August.
[4] H.M.S.Badar Andrews, S. Ahmed, N.I. Kajla, G. Fan, C. Zhang, Q-BLAISE: quantum-resilient blockchain and AI-enhanced security protocol for smart grid IoT, IEEE Trans. Consum. Electron. 71 (2) (2025) 4959–4971.
[5] 3GPP, "NR; NR and NG-RAN Overall description; stage 2," 3GPP TS 38.300, ver. 16.2.0, Release 16, Jul. 2020.
[6] M. Nandy, A. Dubey, IoT and 5G integration: transforming real-time applications in smart industries, in: IEEE, *International Conference on Automation and Computation (AUTOCOM)*, Dehradun, India, 2025, pp. 1207–1211, https://doi.org/10.1109/AUTOCOM64127.2025.10957077.
[7] F. Yin, Q. Liu, M. Chen, Y. Hu, L. Jin, S. Li, Resource allocation for heterogeneous services in satellite-terrestrial IoT networks with multi-access edge computing, IEEE Trans. Wirel. Commun. 25 (2026) 11980–11997, https://doi.org/10.1109/TWC.2026.3662769.
[8] S.H. Abdelwahed, I.M. Hefny, M. Hegazy, L.A. Said, A. Soltan, Survey of IoT multi-protocol gateways: architectures, protocols and cybersecurity, Internet Things 33 (2025) 101703, https://doi.org/10.1016/j.iot.2025.101703.
[9] B. Padma, S.B. Erukala, End-to-end communication protocol in IoT-enabled ZigBee network: investigation and performance analysis, Internet Things 22 (2023) 100796, https://doi.org/10.1016/j.iot.2023.100796.
[10] G. Mantilla, A. I, F. Meyer, V. Turau, A comprehensive performance comparison of IEEE 802.15.4 DSME and TSCH in a realistic IoT scenario for industrial applications, ACM Trans. Internet Things 4 (3) (2023) 1–30, https://doi.org/10.1145/3595188. Article 16.
[11] D. Guglielmo, S. Brienza, G. Anastasi, IEEE 802.15.4e: a survey, Comput. Commun. 88 (2016) 1–24, https://doi.org/10.1016/j.comcom.2016.05.004.
[12] P. Alemany, et al., Defining intent-based service management automation for 6G multi-stakeholders scenarios, IEEE Open J. Commun. Soc. 6 (2025) 2373–2396, https://doi.org/10.1109/OJCOMS.2025.3554250.
[13] J. Wang, et al., Hierarchical index retrieval-driven wireless network intent translation with LLM, IEEE Trans. Mob. Comput. 24 (10) (2025) 9837–9851, https://doi.org/10.1109/TMC.2025.3564937.
[14] A. Nosratinia, T.E. Hunter, A. Hedayat, Cooperative communication in wireless networks, IEEE Commun. Mag. 42 (10) (2020) 74–80, https://doi.org/10.1109/MCOM.2004.1341264.
[15] N. Li, W. Mei, P. Wu, B. Ning, L. Zhu, Movable antenna enhanced DF and AF relaying systems: performance analysis and optimization, IEEE Trans. Commun. 73 (12) (2025) 13239–13255, https://doi.org/10.1109/TCOMM.2025.3593660.

[16] F. Wang, J. Xu, V.K.N. Lau, S. Cui, Amplify-and-forward relaying for hierarchical over-the-air computation, IEEE Trans. Wirel. Commun. 21 (12) (2022) 10529–10543, https://doi.org/10.1109/TWC.2022.3185074. Dec.

[17] W. Wu, W. Wang, R. Song, Coexisting RIS induced multipath fading in high-speed train systems, IEEE Trans. Veh. Technol. (2025) 1–14, https://doi.org/10.1109/TVT.2025.3567822.

[18] X. Liang, Q. Liu, W. Cao, S. Liu, X. Zhao, AoI Minimization for RIS-Assisted V2V Relay System With Deep Reinforcement Learning, IEEE Internet Things J. 12 (14) (2025) 27450–27460, https://doi.org/10.1109/JIOT.2025.3564334, 15.

[19] X. Qu, Z. Shang, G. Qiao, Y. Zhou, Location-aided maximal ratio combining for an acoustic vector sensor in multipath channels, IEEE Signal Process. Lett. 32 (2025) 3300–3304, https://doi.org/10.1109/LSP.2025.3597557.

[20] A.J. Bhuvaneshwari, P. Kaythry, A review of deep learning strategies for enhancing cybersecurity in networks, J. Sci. Ind. Res. 82 (12) (2023) 316–1330, https://doi.org/10.56042/jsir.v82i12.1702.

[21] A.J. Bhuvaneshwari, P. Kaythry, Secure IoV communications for smart fleet systems empowered with ASCON, Sci. Rep. 15 (1) (2025) 19103, https://doi.org/10.1038/s41598-025-04061-w.

[22] X. Zheng, A. Leivadeas, M. Falkner, Intent based networking management with conflict detection and policy resolution in an enterprise network, Comput. Netw. 219 (2022) 109457, https://doi.org/10.1016/j.comnet.2022.109457.

[23] P. Kumar, N. Goel, M. Tolani, S. Kamath, UAV-assisted superposition coded cooperation: hybrid relaying and nakagami- m channel for UL/DL, IEEE Access 13 (2025) 58108–58119, https://doi.org/10.1109/ACCESS.2025.3555120.

[24] T. Yuan, M. Liu, Y. Feng, Performance of SWIPT cooperative DF communication systems with hybrid receiver and non-linear energy harvesting model, Sensors (2020) 1–13, https://doi.org/10.3390/s20092472.

[25] F.A. Semire, C.K. Agubor, A.O. Akande, O.K. Akinde, Z.K. Adeyemo, Intelligent empirical model for interference mitigation in 5G mobile network at Sub6 GHz transmission frequency, Int. J. Wirel. Inf. Netw. (Springer) 2 (5) (2023), https://doi.org/10.1007/s10776-023-00603-z.

[26] Y. Sun, J. Wu, W. Wu, J. Xu, Deep reinforcement learning-based cooperative relay selection for NOMA systems, J. Beijing Inst. Technol. 33 (2) (2024) 116–126. https://journal.hep.com.cn/jbit/EN/10.15918/j.jbit1, 004-0579.2024.116.

[27] O.K. Akinde, O.A. Akande, C. Etus, O.J Odeyinka, Development of a modified empirical model for new mobile radio network at 28 GHz millimeter wave spectrum, LAUTECH J. Eng. Technol. 16 (1) (2022) 52–59.

[28] M.A. Al-Shareeda, T. Gaber, M.A. Alqarni, M.H. Alkinani, A.A. Almazroey, A.A. Almazroi, Chebyshev polynomial based emergency conditions with authentication scheme for 5G-assisted vehicular fog computing, IEEE Trans. Dependable Secure Comput. 22 (5) (2025) 4795–4812, https://doi.org/10.1109/TDSC.2025.3553868. Sept.-Oct.

[29] B.A. Mohammed, M.A. Al-Shareeda, S. Manickam, Z.G. Al-Mekhlafi, A.M. Alayba, A.A. Sallam, ANAA-Fog: a novel anonymous authentication scheme for 5G-enabled vehicular Fog computing, Mathematics 11 (6) (2023) 1446, https://doi.org/10.3390/math11061446.

[30] M.A. Al-Shareeda, M. Anbar, S. Manickam, I.H. Hasbullah, Password-guessing attack-aware authentication scheme based on Chinese Remainder Theorem for 5G-enabled vehicular networks, Appl. Sci. 12 (3) (2022) 1383, https://doi.org/10.3390/app12031383.

[31] A.A. Almazroi, E.A. Aldhahri, M.A. Al-Shareeda, S. Manickam, ECA-VFog: an efficient certificateless authentication scheme for 5G-assisted vehicular fog computing, PLoS ONE 18 (6) (2023) e0287291, https://doi.org/10.1371/journal.pone.0287291.

[32] M.A. Al-Shareeda, S. Manickam, B.A. Mohammed, Z.G. Al-Mekhlafi, A. Qtaish, A.J. Alzahrani, G. Alshammari, A.A. Sallam, K. Almekhlafi, CM-CPPA: chaotic map-based conditional privacy-preserving authentication scheme in 5G-enabled vehicular networks, Sensors 22 (13) (2022) 5026, https://doi.org/10.3390/s22135026.

[33] M.A. Al-Shareeda, S. Manickam, B.A. Mohammed, Z.G. Al-Mekhlafi, A. Qtaish, A.J. Alzahrani, G. Alshammari, A.A. Sallam, K. Almekhlafi, Provably secure with efficient data sharing scheme for fifth-generation (5G)-enabled vehicular networks without road-side unit (RSU), Sustainability 14 (16) (2022) 9961, https://doi.org/10.3390/su141699613.

[34] M.S. Al-Kahtani, A review of relay assignment problem in cooperative wireless sensor networks, Electronics 9 (3) (2020) 443, https://doi.org/10.3390/electronics9030443.

[35] P.T. Lucero, H. Carvajal Mora, N. Orozco Garzón, F. Almeida García, On the performance of decode-and-forward equal-gain-combining relay systems over Weibull fading channels, Sensors 23 (6) (2023) 3174, https://doi.org/10.3390/s23063174.

[36] C. Song, Y. Wang, Y. Zhou, et al., Performance analysis of shared relay CR-NOMA network based on SWIPT, EURASIP J. Wirel. Commun. Netw. (2024), https://doi.org/10.1186/s13638-024-02398-w. Article 70.

[37] H.Q. Tran, X.Q. Le, Full-duplex cooperative relaying systems for simultaneous wireless information and power transfer with non-orthogonal multiple access, Digit. Signal Process. 156 (2025) 104817, https://doi.org/10.1016/j.dsp.2024.104817. B.

[38] D. Kim, M.R. Castellanos, R.W. Heath Jr., Joint relay selection and beam management based on deep reinforcement learning for millimeter-wave vehicular communication, IEEE Trans. Veh. Technol. 72 (10) (2023) 13067–13080, https://doi.org/10.1109/TVT.2023.3274763.

[39] J. Qian, H. Li, P. Zhu, A. Zhou, S. Liu, F. Wang, Cooperative jamming and relay selection for covert communications based on reinforcement learning, Sensors 25 (19) (2025) 6218, https://doi.org/10.3390/s25196218.

[40] Luo, J., Sampath, A., Abedini, N., and Luo, T., Performance study of various relay nodes in 5G wireless network. *arXiv preprint arXiv*:2024, 45–56, https://arxiv.org/abs/2407.20089.

[41] M.K. Simon, M.-S. Alouini, Digital Communication Over Fading Channels, 2nd ed., John Wiley & Sons, Hoboken, NJ, 2005.

[42] T.S. Rappaport, Wireless Communications: Principles and Practice, Cambridge University Press, Cambridge, UK, 2024, p. 116.

[43] D.C. Montgomery, G.C. Runger, Applied Statistics and Probability for Engineers, 7th ed., Wiley, 2018.

[44] H. Nie, Y. Wu, W. Zhu, J. Zhong, H. Yang, Y. Zhou, Time-triggered task offloading scheduling in TSN-based edge computing power networks, IEEE Access 13 (2025) 85979–85996, https://doi.org/10.1109/ACCESS.2025.3568848.

[45] S. Kou, C. Yang, M. Gurusamy, SAFLA: semantic-aware full lifecycle assurance for intent-driven networks, IEEE Trans. Cogn. Commun. Netw. 12 (2026) 658–672, https://doi.org/10.1109/TCCN.2025.3565592.

[46] B. Tang, L. Huang, Q. Li, A. Pandharipande, X. Ge, Cooperative semantic communication with on-demand semantic forwarding, IEEE Open J. Comm. Soc. 5 (2024) 349–363.

[47] K.C. Okafor, et al., Mitigating COVID-19 spread in closed populations using networked robots and Internet of Things, IEEE Internet Things J. 11 (24) (2024) 39424–39434, https://doi.org/10.1109/JIOT.2024.3431874.

[48] M.R. Garcia, Millimeter Wave Spectrum For 5G, IEEE Press, 2019, https://doi.org/10.1109/MCOM.2019.1800714.

[49] Y.-R. Tsai, H.-Y. Liu, On the Feasibility and optimization of providing delay sensitive services based on bluetooth low energy advertising technology, IEEE Access 13 (2025) 149010–149019, https://doi.org/10.1109/ACCESS.2025.3601116.

[50] L. Scalambrin, A. Zanella, X. Vilajosana, A lightweight algorithm for efficient synchronization in LoRaWAN class-B networks, IEEE Internet Things J. 12 (16) (2025) 32749–32764, https://doi.org/10.1109/JIOT.2025.3582443, 15.

[51] R. Deepa, V.P. Harigovindan, V. Goutham, S. Kalathil, Enhanced SWIPT with cooperative relaying for energy efficient and reliable NOMA-based underwater acoustic sensor networks, IEEE Access 13 (2025) 142089–142102, https://doi.org/10.1109/ACCESS.2025.3588063.

[52] K.C. Okafor, B. Adebisi, K. Anoh, Lightweight multi-hop routing protocol for resource optimisation in edge computing networks, Internet Things 22 (2023) 100758, https://doi.org/10.1016/j.iot.2023.100758.

[53] Y. Huang, Y. Zhao, Z. Chen, H. Zhang, J. Lv, X. Qiao, Intent-driven cognitive XR networks: multi-agent orchestration for immersive communication, IEEE J. Sel. Areas Commun. 44 (2026) 3137–3151, https://doi.org/10.1109/JSAC.2025.3649618.

[54] M.A. Habib, et al., Harnessing the power of LLMs, informers and decision transformers for intent-driven RAN management in 6G, IEEE Trans. Netw. Sci. Eng. 13 (2026) 4187–4206, https://doi.org/10.1109/TNSE.2025.3596028.

[55] D. Wang, S. Zou, M. Liwang, W. Ni, X. Wang, Intent-driven cognitive xDFC bridge in endogenous intelligent IIoT: a systematic review and S2Croft architecture with Bayesian-CRO-fuzzy synergy, IEEE Trans. Netw. Sci. Eng. 13 (2026) 1026–1042, https://doi.org/10.1109/TNSE.2025.3589594.

[56] Y. Wang, C. Yang, T. Li, Y. Ouyang, X. Mi, Y. Song, A survey on intent-driven end-to-end 6G mobile communication system, IEEE Commun. Surv. Tutor. 28 (2026) 882–915, https://doi.org/10.1109/COMST.2025.3575041.
[57] M. Sadiq, M.S. Haider, A. Fatima, M.S.J. Solaija, H. Jung, S.A. Hassan, Intent-driven hierarchical DRL for secrecy-aware AoI–AoLI optimization in RIS-assisted HAP-IoT communications, IEEE Internet Things J. (2025), https://doi.org/10.1109/JIOT.2025.3648959.
[58] K.C. Okafor, B. Adebisi, A.O. Akande, K. Anoh, Agile gravitational search algorithm for cyber-physical path-loss modelling in 5G connected autonomous vehicular network, Veh. Commun. 45 (2024) 100685, https://doi.org/10.1016/j.vehcom.2023.100685.